Tellus (2002), 54B, 784–819
Printed in UK. All rights reserved

TELLUS
ISSN 0280–6509

A simple three-dimensional canopy – planetary boundary layer simulation model for scalar concentrations and fluxes

By ANDREJ SOGACHEV[1,2]*, GENNADY V. MENZHULIN[3], MARTIN HEIMANN[1] and JON LLOYD[1],
[1]*Max Planck Institute for Biogeochemistry, Postfach 100164, 07701 Jena, Germany;* [2]*Severtsov Institute of Ecology and Evolution, Russian Academy of Sciences, Leninsky Prospect 33, 117071, Moscow, Russia;* [3]*Center for International Environmental Cooperation, Russian Academy of Sciences, em. Kutuzova 14, 191187, St. Petersburg, Russia*

(Manuscript received 2 July 2001; in final form 17 June 2002)

ABSTRACT

We present a numerical model capable of computing the physical processes within both plant canopy and planetary boundary layer (PBL), offering the potential benefit of wide applicability due to reduced computational requirements. The model, named SCADIS (scalar distribution), synthesizes existing knowledge of boundary and surface layer turbulence and surface layer vegetative processes and was tested using several data sets from the European part of Russia and Siberia obtained as part of the EUROSIBERIAN CARBONFLUX project. Despite simplifications which were necessary in order to simulate the natural processes, the first version of the model presented here demonstrated a satisfactory agreement between modelled and observed data for different surface features and weather conditions. For example, the model successfully predicted the diurnal patterns of concentration profiles of CO_2, water vapour and potential temperature profiles both within the summer atmospheric boundary layer and within the plant canopy itself. The very different effects of the surface energy characteristics of bog versus forest on convective boundary layer (CBL) structure and development are also illustrated. The model was applied to evaluate the effective footprints for eddy covariance measurements above non-uniform plant canopies, the case study here being a mixed spruce forest in European Russia. The model also demonstrates the likely variations in the above-canopy turbulence and surface layer fluxes as dependent on the presence of patches of deciduous broadleaf forest within a predominantly evergreen coniferous stand.

1. Introduction

Both the canopy microclimate and the atmospheric environment above are strongly influenced by the fundamental exchange processes of momentum, energy and matter that occur in the presence of soil and vegetation over much of the earth's surface. These influences range over many scales: from the effects of isolated trees on the temperature and hydrological regimes of the canopy and soil below them (Belsky et al., 1989), to the influence of canopy structure and energy fluxes on within-canopy profiles of momentum and other entities (Raupach et al., 1996; Finnigan, 2000) and regional-scale processes such as planetary boundary layer (PBL) dynamics (Raupach, 1995).

In order to simulate these processes, different types of models have been proposed. One common model type describes processes in the surface boundary layer only: the so-called Soil–Vegetation–Atmosphere Transfer (SVAT) models. The complexity of SVAT models ranges from the simple big-leaf models to multilayer models with higher-order closure formulation of the turbulent transport within and above the

*Corresponding author.
e-mail: sogachev@bgc-jena.mpg.de

vegetation (Ayotte et al., 1999; Kanda and Hino, 1994; Mix et al., 1994; Nichols, 1992; Sellers et al., 1986; Wilson, 1988; Wu et al., 2000; Zeng and Takahashi, 2000). As a rule, the parameterization schemes of such models require as input data many parameters representing the properties of the land surface. However, many theoretical and numerical problems that occur in multi-dimensional boundary layer modelling are of only secondary interest for those seeking solutions to more applied problems. This is one reason that mathematically closed models of boundary layer turbulent flow and meso-meteorological regime that also include a spatially explicit vegetation layer are rare. They are represented, in general, by two-dimensional simplified models (e.g. Tsipris and Menzhulin, 1972; Dubov and Bykova, 1973; Dubov et al., 1978), dynamic models for the description of shelterbelts and windbreaks effects (Wilson and Flesch, 1999; Liu et al., 1996; Schilling, 1991; Wang et al., 2001; Zhenjia et al., 1990) and non-universal complex meso-meteorological models of the type developed by Gross (1987; 1993) or limited area LES-models (Shaw and Schumann, 1992; Shen and Leclerc, 1997).

To overcome computational problems, most planetary boundary layer (PBL) models using SVAT schemes tend to rely solely on simple empirical formulations (Kunz and Moussiopoulos, 1995; Pielke, 1984). However, several studies have shown that variations in surface characteristics can affect the prediction of near-surface turbulent fluxes in the PBL (Alapaty et al., 1997; Garratt et al., 1996; Sun and Bosilovich, 1996; Gross, 1993). These variations in the turbulent fluxes might be expected to influence the prediction of PBL structure. Thus, in the current context it was deemed desirable to develop a mathematical model of meso-meteorological processes incorporating two important characteristics simultaneously. On the one hand the model was envisaged to be able to describe in a realistic manner physical processes forming the meteorological regime within and above the forest canopy; such is typically the case for SVAT models. On the other hand, it was also designed so as to allow a realistic description of PBL processes without resort to vast computing expenses.

A model satisfying such properties would have the potential to be widely applied if it could resolve with sufficient reliability many questions concerning the advective contribution to fluxes measured by either gradient or eddy-correlation methods in the presence of some vegetation heterogeneity. During the EUROSIBERIAN CARBONFLUX project, some measurements were carried out on towers located in forests not characterized by homogeneous and uniform vegetation in all directions and for some considerable distance. Analytical methods for an estimation of upwind fetch were not sufficient to explain problems in the closure of the observed energetic balance and to describe the contribution of various sources to the observed scalar fluxes. Therefore the main purpose of our work here was the development of a numerical tool, which would help in the interpretation of experimental data and improve our understanding of processes in canopy – planetary boundary layer interactions. The model described below and named SCADIS (scalar distribution) is the first version of this tool. It synthesizes existing knowledge of boundary and surface layer turbulence and surface layer vegetative processes. The model is tested using several data sets obtained as part of the EUROSIBERIAN CARBONFLUX project.

The paper is organized as follows. In Section 2 equations of the model, its domain and both boundary and initial conditions are formulated. In Section 3 a brief review is given of experimental sites from which data were used for model testing. Section 4 presents comparisons between one-dimensional model results and observed data and also results of two- and three-dimensional numerical experiments. Both weak and strong characteristics of the model are also discussed in Section 4. A number of potential applications for the model are outlined in the conclusion. Appendices present all model equations that are not described in Section 2.

2. Model description

In this section the basic equations of models describing transfer, sources and sinks of momentum, heat, humidity and carbon dioxide in the atmosphere as well as the prognostic equations for moisture in soil are presented. The turbulence closure is then discussed, following which the concepts of radiation description in the model, based on important features of the radiation regime within and above the canopy, are defined. Finally the boundary and initial conditions of the model together with some numerical aspects are considered.

To simplify the presentation some equations are included only in the appendices. All equations that have been used to calculate the radiation fluxes within and above the vegetation are given in Appendix A. Energy balance equations for leaves are given in Appendix B. Appendix C is devoted to conditions at the bottom and upper borders of the model. The expression for calculations of integral coefficients of heat, water vapour and carbon dioxide exchange between the leaves and the canopy air are described in Appendix D.

2.1. Basic equations

The model SCADIS is based on the Reynolds equations for turbulent flow, obtained by well known transformations of the Navier–Stokes equations (Monin and Yaglom, 1965). Turbulent fluxes are expressed as the product of turbulent diffusion coefficient and the gradient of a mean quantity according to ideas first proposed by Boussinesq (Vager and Nadezhina, 1979; Penenko and Aloyan, 1985; Sorbjan, 1989). Furthermore, we ignore the small spatial temporary changes of air density that occur within the atmospheric boundary layer (Gutman, 1969), this allows considerable simplification of the equations by the exclusion of terms defining gradients in air density and pressure. According to these assumptions the momentum equations within and above vegetation canopy are:

$$\frac{\partial u}{\partial t} + u\frac{\partial u}{\partial x} + v\frac{\partial u}{\partial y} + w\frac{\partial u}{\partial z} = f(v - v_g) + \frac{\partial}{\partial x}K_x\frac{\partial u}{\partial x} + \frac{\partial}{\partial y}K_y\frac{\partial u}{\partial y} + \frac{\partial}{\partial z}K_z\frac{\partial u}{\partial z} - c_d s\sqrt{(u^2+v^2+w^2)}u, \tag{1}$$

$$\frac{\partial v}{\partial t} + u\frac{\partial v}{\partial x} + v\frac{\partial v}{\partial y} + w\frac{\partial v}{\partial z} = -f(u - u_g) + \frac{\partial}{\partial x}K_x\frac{\partial v}{\partial x} + \frac{\partial}{\partial y}K_y\frac{\partial v}{\partial y} + \frac{\partial}{\partial z}K_z\frac{\partial v}{\partial z} - c_d s\sqrt{(u^2+v^2+w^2)}v,$$

combined with the continuity equation, viz.

$$\frac{\partial u}{\partial x} + \frac{\partial v}{\partial y} + \frac{\partial w}{\partial z} = 0, \tag{2}$$

where axes x and y are directed to the east and to the north correspondingly, z is the local vertical axis, t represents time, u, v and w are the velocity components along the x, y and z axes, respectively, u_g and v_g are the components of geostrophical wind (over the atmospheric boundary layer), f is the Coriolis parameter, K is the turbulent diffusion coefficient of momentum (subscripts x, y and z denote components in the corresponding directions), s is the projected leaf surface area density and c_d is the drag coefficient for unit plant area density.

In natural conditions, leaves and other phytoelements are differentially illuminated by the incoming solar radiation. Some parts of the vegetative canopy are shaded by leaves or stems located higher up, whereas other elements lower down may be exposed to direct radiation in the form of sun-flecks. This results in a complex distribution of both radiation and temperature on the canopy surface. This temperature is mosaic in character, and it is not easily described by a single temperature parameter. In more detailed models of canopy microclimates, four thermal characteristics are defined (i.e. separate temperatures for the adaxial and abaxial surfaces of both the sunlit and shaded portions within the canopy). However, such complexity may not be necessary as there are calculations which show that the differences in temperatures between the abaxial and adaxial leaf surface under the conditions of identical illumination appear trivially small (Menzhulin, 1986). It is probably sufficient then to develop a model with only two temperatures describing the heat regime of phytomass, these being the temperatures of sunlit, T_l^{sn}, and shaded, T_l^{sd}, surfaces of the vegetation surface. Associated with these different canopy temperatures are different humidities of air within the stomatal cavities q_l^{sn} and q_l^{sd}. Equations for heat and water vapor transfer between the vegetation and the atmospheric boundary layer can then be written:

$$\frac{\partial T}{\partial t} + u\frac{\partial T}{\partial x} + v\frac{\partial T}{\partial y} + w\frac{\partial T}{\partial z} = \frac{\partial}{\partial x}K_{x\mathrm{H}}\frac{\partial T}{\partial x} + \frac{\partial}{\partial y}K_{y\mathrm{H}}\frac{\partial T}{\partial y} + \frac{\partial}{\partial z}\alpha_\mathrm{H}K_z\left(\frac{\partial T}{\partial z} + \gamma_\mathrm{a}\right) + s_\mathrm{H}\left[\eta g_\mathrm{H}^{sn}\left(T_l^{sn} - T\right) + (1-\eta)g_\mathrm{H}^{sd}\left(T_l^{sd} - T\right)\right] + \frac{1}{\rho_\mathrm{a}C_p}\frac{\partial}{\partial z}\left(R_\mathrm{LWR}^{\downarrow} - R_\mathrm{LWR}^{\downarrow}\right) \tag{3}$$

and

$$\frac{\partial q}{\partial t} + u\frac{\partial q}{\partial x} + v\frac{\partial q}{\partial y} + w\frac{\partial q}{\partial z} = \frac{\partial}{\partial x}K_{x\mathrm{V}}\frac{\partial q}{\partial x} + \frac{\partial}{\partial y}K_{y\mathrm{V}}\frac{\partial q}{\partial y} + \frac{\partial}{\partial z}\alpha_\mathrm{V}K_z\frac{\partial q}{\partial z} + s_\mathrm{V}\left[\eta g_\mathrm{V}^{sn}\left(q_l^{sn} - q\right) + (1-\eta)g_\mathrm{V}^{sd}\left(q_l^{sd} - q\right)\right]. \tag{4}$$

In eq. (3) $R_{\rm LWR}^{\downarrow}$ and $R_{\rm LWR}^{\uparrow}$ describe the upward and downward longwave radiation fluxes without vegetation, respectively, $\rho_{\rm a}$ is the air density, C_p is the specific heat of dry air at constant pressure, $\gamma_{\rm a}$ is the dry adiabatic lapse rate ($\gamma_{\rm a} = 0.0098$ K m^{-1}), T is air temperature and $\alpha_{\rm H}$ is the converse Prandtl number. In eq. (4) q is air specific humidity and $\alpha_{\rm V}$ is the converse Schmidt number for water vapour. Based on the conclusions of Legotina and Orlenko (1977), an equality of turbulent coefficients for heat and passive tracer transfer, i.e. $\alpha = \alpha_{\rm H} = \alpha_{\rm V}$, is assumed. Due to the empirical dependence of these coefficients on the Richardson number (Ri) we therefore approximate them by the following empirical formulations (Businger et al., 1971):

$$\alpha(Ri) = \begin{cases} 1.35 & \text{for} \quad Ri \geq 0 \\ 1.35(1 - 15Ri)^{1/4} & \text{for} \quad Ri < 0. \end{cases} \tag{5}$$

In the eqs. (3) and (4) subscripts H and V refer to heat and water vapour, respectively, $g_{\rm H}^{sn}$, $g_{\rm H}^{sd}$, $g_{\rm V}^{sn}$ and $g_{\rm V}^{sd}$ are the integral exchange coefficients for heat and water vapour between the canopy air and phytoelement surfaces (see Appendix D), η is the sunlit vegetation surface area fraction (see Section 2.3 and Appendix A) and $s_{\rm H}$ and $s_{\rm V}$ are the total leaf surface area densities taking part in heat and moisture exchange with surrounding air, respectively. In general, the relationship between s and both $s_{\rm H}$ and $s_{\rm V}$ depends on the vegetation type. In our model we assume $s_{\rm H} = s_{\rm V} = 2.7s$ for coniferous and $s_{\rm H} = s_{\rm V} = 2s$ for deciduous vegetation (Varlagin and Vygodskaya, 1993). In the present study special cloud physics effects have been ignored.

For the transfer of a passive tracer, in this case carbon dioxide, we use an equation analogous to (4):

$$\begin{aligned} \frac{\partial C}{\partial t} + u\frac{\partial C}{\partial x} + v\frac{\partial C}{\partial y} + w\frac{\partial C}{\partial z} &= \frac{\partial}{\partial x}K_{x\rm V}\frac{\partial C}{\partial x} \\ &+ \frac{\partial}{\partial y}K_{y\rm V}\frac{\partial C}{\partial y} + \frac{\partial}{\partial z}\alpha K_z\frac{\partial C}{\partial z} \\ &+ s_{\rm V}\left[\eta g_{\rm C}^{sn}\left(C_l^{sn} - C\right) + (1-\eta)g_{\rm C}^{sd}\left(C_l^{sd} - C\right)\right]. \end{aligned} \tag{6}$$

Here C is the atmospheric CO_2 concentration, and C_l^{sn} and C_l^{sd} are accordingly the CO_2 concentrations in the intercellular spaces of the sunlit and shaded parts of the leaf. $g_{\rm C}^{sn}$ and $g_{\rm C}^{sd}$ are the integral exchange coefficients for carbon dioxide between the canopy air and phytoelement surfaces (see Appendix D). The intercellular mole fraction of CO_2 is calculated here according to the model of Lloyd and Farquhar (1994), which is in turn based on the ideas of Cowan (1977):

$$C_l^{sn,sd} = C\left(1 - \sqrt{\frac{1.6D^{sn,sd}(C - \Gamma^{sn,sd})}{\lambda C^2}}\right), \tag{7}$$

where $D^{sn,sd}$ is the leaf-to-air vapour mole fraction difference and $\Gamma^{sn,sd}$ is the compensation mole fraction of CO_2 for the sunlit and shaded parts of the canopy taken as $2.0T_l^{sn,sd}$ accordingly. λ is a Lagrange multiplier representing the marginal water cost of plant carbon gain (Cowan, 1977; Cowan and Farquhar, 1977). λ for the C_3 plants of different biomes has been estimated by Lloyd and Farquhar (1994). The plant respiration is not described in the present model. The rate of soil respiration is determined by the features of the uppermost soil layer and ground surface temperature [see eq. (C7) in Appendix C].

One of the most important characteristics of any underlying surface is its water content. Since the presented model is three-dimensional, the calculations are highly time consuming and that is why we chose the parameterisation proposed by Noilhan and Planton (1989) to describe the processes of water transport in soil. Here are two soil layers to represent the surface and subsurface processes; layer 1 is 0.01 m thick and layer 2 is 1 m thick. The prognostic equations for the superficial moisture $w_{\rm g}$ (layer 1), and the bulk soil moisture w_2 (layer 2) are given as

$$\frac{\partial w_{\rm g}}{\partial t} = \frac{C_1}{\rho_{\rm w} d_1}(P_{\rm g} - E_{\rm g}) - \frac{C_2}{t_{\rm day}}(w_{\rm g} - w_{\rm geq}) \tag{8}$$

and

$$\frac{\partial w_2}{\partial t} = \frac{1}{\rho_{\rm w} d_2}(P_{\rm g} - E_{\rm g} - E_{\rm tr}), \tag{9}$$

where $t_{\rm day}$ is a time constant of one day, $\rho_{\rm w}$ is the density of liquid water, d_1 and d_2 are the thicknesses of the two soil layers, $P_{\rm g}$ is the flux of liquid water reaching the soil surface (precipitation), $E_{\rm g}$ is the evaporation from the soil surface, and $E_{\rm tr}$ is the transpiration from the vegetation. The hydraulic coefficients C_1 and C_2 and the equilibrium value $w_{\rm geq}$ are expressed as functions of soil texture and soil moisture. For further details, see Noilhan and Planton (1989) and Jacquemin and Noilhan (1990).

For the short-term simulation here, we ignore evaporation of intercepted water by the canopy.

2.2. Turbulence closure

It is sometimes assumed that an improvement in results is a necessary consequence of the use of a more complex model. However, this need not always be the case, especially if added complexity leads to problems of reliability, or if the results are particularly sensitive to uncertain parameterizations (Brown, 1996). Therefore, in deciding on a method to obtain closure of the boundary layer equation system, we have taken into account considerations other than a desire to obtain new and reliable information on the structure of turbulent flow. We use an one-and-a-half order closure procedure with the equation of turbulent energy transfer (Monin and Yaglom, 1965; Menzhulin, 1986; Stull, 1988):

$$\frac{\partial e}{\partial t} + u\frac{\partial e}{\partial x} + v\frac{\partial e}{\partial y} + w\frac{\partial e}{\partial z} = K_z\left[\left(\frac{\partial u}{\partial z}\right)^2 + \left(\frac{\partial v}{\partial z}\right)^2 + \left(\frac{\partial w}{\partial z}\right)^2 - \alpha\frac{g}{T_0}\left(\frac{\partial T}{\partial z} + \gamma_a\right) - \alpha\frac{0.618}{\rho_a}g\frac{\partial q}{\partial z}\right] + \frac{\partial}{\partial x}K_x\frac{\partial e}{\partial x} + \frac{\partial}{\partial y}K_y\frac{\partial e}{\partial y} + \frac{\partial}{\partial z}\alpha_e K_z\frac{\partial e}{\partial z} - \varepsilon + c_d s(\sqrt{u^2+v^2+w^2})^3 - 4c_d s e\sqrt{u^2+v^2+w^2}. \tag{10}$$

In this equation e is turbulence intensity, g is the acceleration of gravity constant, ε is the dissipation of turbulent energy, T_0 is the local potential temperature at level z and $\alpha_e = 0.73$ is the converse Schmidt number for turbulent energy. For continuation of the closure procedure we also use the Kolmogorov (1941; 1942) hypothesis and suppose that

$$K_z = c^{1/4} l_e \sqrt{e}, \tag{11}$$

$$\varepsilon = c^{3/4} e^{3/2} / l_\varepsilon. \tag{12}$$

In eqs. (11) and (12) l_e is the turbulence length scale, l_ε is the dissipation length scale and c is a dimensionless empirical constant equal to 0.046. Many studies have been devoted to the definition of a length scale because the successful representation of this variable can, in many respects, improve the modelled distribution of other parameters of turbulent flow in the whole boundary layer (Therry and Lacarrere, 1983; Carroll, 1993; Apsley and Castro, 1997; Ziemann, 1998). In the present model we opt for simplicity and accept the well known assumption of an equality in scale for eqs. (11) and (12). That is to say, $l = l_e = l_\varepsilon$. We note, however, that a number of authors have specified the necessity to use different scales for dissipation and for the size of mixing in a stratified atmosphere (e.g. Therry and Lacarrere, 1983). In our case, expression (12) is thus rewritten as

$$\varepsilon = ce^2 \big/ K_z.$$

The commonly used ratios for turbulence scales allow us to define l via the local average characteristics of a driven flow (Laykhtman, 1970; Zilitinkevitch, 1970). Specifics of turbulence scale l formation inside the vegetation canopy (Menzhulin, 1970; 1974) are taken into account by means of the following equations:

$$\frac{1}{l} = \frac{s}{0.40 d_f} + \frac{1}{l_{LZ}}, \qquad l_{LZ} = -0.40\frac{\psi}{(\partial\psi/\partial z)}, \qquad \psi = \frac{\sqrt{e}}{l_{LZ}}. \tag{13}$$

Here l_{LZ} is the turbulence scale of Laykhtman–Zilitinkevitch, 0.40 is the von Karman constant and d_f is an empirical dispersion parameter for the foliage. Equation (13) shows that turbulence within dense vegetation is characterized by a length scale which is dependent on the "cell" volume (size) between vegetative elements. Its magnitude decreases with increasing foliage density and consequently the specific surface s. When $s \to 0$, the influence of soil surface on l increases. Then l depends on ψ only.

It has been shown that the eq. (13) has some limitations (Bobylyeva, 1970; Vager and Nadezhina, 1979). Those authors concluded that this expression results in the turbulence coefficient being strongly overestimated near the top of the boundary layer. To circumvent this problem we have therefore modified the first part of eq. (13) following Blackadar (1962), using a basic mixing length l_0:

$$l = \left(\frac{s}{0.40 d_f} + \frac{1}{l_{LZ}} + \frac{1}{l_0}\right)^{-1}. \tag{14}$$

To establish a dependence of a structure of the turbulence scale not only on parameters at the top of the boundary layer but also on structure within most of the boundary layer is convenient in this case. We thus use the expression for l_0 offered by Mellor and Yamada (1975), viz.

$$l_0 = \alpha_1 \int_0^{z_i} \sqrt{e}\cdot z\,\mathrm{d}z \Big/ \int_0^{z_i} \sqrt{e}\,\mathrm{d}z. \tag{15}$$

Here $\alpha_1 = 0.2$ is an empirical constant and z_i is the height of the convective boundary layer (CBL).

To calculate the horizontal turbulent coefficients K_x and K_y we used the semi-empirical formula first offered by Smagorinsky (1965), viz.

$$K_x = K_y = \frac{0.40^2}{2}\left|\sqrt{\left(\frac{\partial u}{\partial x} - \frac{\partial v}{\partial y}\right)^2 + \left(\frac{\partial v}{\partial x} + \frac{\partial u}{\partial y}\right)^2}\right| \delta x \delta y. \quad (16)$$

The typical horizontal length scales δx and δy in the finite difference model equations are replaced in the model by the appropriate lengths of horizontal mesh widths. This formulation has been included in our model with the horizontal turbulent coefficients for heat $K_{x\mathrm{H}}$, $K_{y\mathrm{H}}$ and passive tracers $K_{x\mathrm{V}}$, $K_{y\mathrm{V}}$ related to that for momentum through the converse turbulent Prandtl and Schmidt numbers, respectively, a value of 1.35 being used here for these numbers.

2.3. *Radiation parameterization and energy balance equations*

Within each gridcell the description of radiation transfer in SCADIS is based on an idealized structure where the canopy is viewed as consisting of many single layers of a horizontally homogeneous and optically isotropic turbid medium. Thereby the characteristics of the stand architecture and radiation do not vary within a horizontal layer but depend only on the height. The penetration of radiation through a plant stand is considered to depend on the leaf area density (LAD): other plant parts such as trunks and branches are disregarded. In addition, we also use a few standard simplifications: (a) for both leaves and the underlying ground the reflection coefficients are considered independent of the incident angle of the incoming radiation; (b) the integrated orientation of foliage is considered constant for all vertical layers and (c) the optical properties of the abaxial and adaxial surfaces of leaves are considered identical. Penumbras are also ignored. However, the model considers separately direct and diffuse components of solar (short-wave) radiation, subdivided into two spectral bands [near-infrared radiation (NIR, 700–3000 nm)] and photosynthetically active radiation (PAR, 400–700 nm), as well as longwave or thermal radiation (LWR).

A full calculation of the characteristics of a radiation regime within the canopy is described in detail in Appendix A; important features are summarized here.

2.3.1. Optical properties and architecture of the stand. We allow for the fact that the ability of radiation to penetrate through a vegetative canopy depends substantially on the canopy architecture: this being defined as the distribution of plants on the ground surface as well as the distribution of leaves, their orientations and leaf sizes. Knowledge of the distribution of foliage density is also necessary to describe the dynamic interaction between the atmosphere and vegetation. Radiation interacts with leaves through absorption and scattering, and these processes vary widely in various parts of the spectrum depending on the leaf and on the underlying ground optical properties. Optical properties of the ground surface under the plant canopy are also allowed for in the model here, and are characterized by their reflection coefficient (albedo). The reflection from the ground surface plays an important role in the radiative regime of a plant stand, especially when the vegetation is sparse or when the ground surface is covered by snow. The major properties of forest stands studied here are given in Table 1 (Section 3).

2.3.2. Calculation of the amount and spectral composition of incident solar radiation and longwave cooling rate above vegetation. The amount and spectral composition of solar radiation reaching the upper border of a plant stand depends on astronomical factors [eq. (A1)] and on atmospheric transparency and cloud conditions [eq. (A2)]. This radiation consists of two components: direct solar radiation as a beam of parallel rays reaching the vegetation from the solar disk and diffuse solar radiation scattered in the earth's atmosphere before reaching the vegetation from all directions of the sky. In many studies of atmosphere–vegetation interactions (e.g. Spitters et al., 1986; DePury and Farquhar, 1997; Lloyd et al., 1995) it has been noted that for the correct estimation of surface fluxes it is important to separate the incoming radiation into direct and diffuse components because of their different spectral composition and penetration characteristics. Here, we also make that distinction, performing separate calculations for direct and diffuse radiation components (Table 2 in Appendix A). Although there has been a recent tendency in SVAT modelling to employ "sun/shade" models (DePury and Farquhar, 1997; Wang et al., 1998) in which the canopy is simply divided into two (sunlit and shaded) components, such an approach was not considered applicable here. One of the main aims of our model is to retain the ability to evaluate the full three-dimensional (3-D) canopy flux characteristics and associated changes within the canopy microclimate.

The long-wave radiation flux term on the right-hand side of eq. (3) that describes the cooling rate without vegetation is computed with the following simplifications: (1) for each level in PBL $R^{\downarrow}_{\mathrm{LWR}}$ is a function of air water content and temperature only, thus the empirical formulae for sky emissivity [eqs. (A10) and (A11)] can be used to estimate it; (2)$R^{\uparrow}_{\mathrm{LWR}}$ within PBL is constant and equivalent to upward long-wave radiation flux at the surface [eqs. (A8) and (A9)].

2.3.3. Estimation of radiation fluxes within vegetation. To estimate the distribution of short-wave radiation within the plant canopy we divide the total radiation into three components (Ross, 1975): (i) direct solar radiation flux as a beam of rays penetrating through the gaps in the foliage without appreciable alteration in spectral characteristics and observed in the form of bright sunflecks; (ii) diffuse solar radiation flux penetrating through the gaps without interacting with the foliage (observed as part of the skylight between plants and leaves); (iii) the flux of scattered radiation as a result of the interaction of direct and diffuse radiation with foliage and the ground surface.

The definition of the penetration functions η [eq. (A3)] and μ [eq. (A4)] for direct and diffuse solar radiation, respectively, is a purely geometrical problem and requires no knowledge of the optical properties of foliage elements. Of the three radiation components forming the radiation field within a canopy, the complementary flux of scattered radiation is the most difficult to estimate [eqs. (A5)–(A7)]. In contrast to the first two components, scattered radiation is strongly influenced by the optical properties of leaves, and its pattern is therefore wavelength-dependent. We feel it is necessary to describe this component accurately for the following two reasons: firstly, the effect of scattered radiation on the energy balance of leaves in the middle and lower layers of the canopy is great; and secondly, the calculation of the canopy albedo requires the correct description of the upward flux of scattered radiation. The definition of a vegetation albedo *a priori* is theoretically not correct for our model (with horizontal resolution 20–100 m). This is because the influence of the spatial distribution of plants with different optical properties as well as the effect of understory vegetation are not taken into account. The description of the ground albedo below the canopy has a sounder physical basis.

The long-wave radiation flux can influence air temperatures not only in the vertical but also in the horizontal direction depending on the horizontal structure of the model vegetation. The transfer properties for long-wave radiation in a canopy differ from those applicable for short-wave radiation. In the model here, a single differential equation suffices for the description of this process, since the scattering of long-wave radiation may effectively be neglected. This equation is divided into upward and downward components [eqs. (A8)–(A11)]. For an accurate description of a long-wave radiation regime within a canopy, the presence of leaves with different temperatures and hence with different rates of thermal emission, poses the greatest problem.

To calculate temperature of the foliage in each vertical layer we have used energy balance equations for sunlit [eq. (B1)] and shaded [eq. (B2)] foliage, respectively (Appendix B). The air humidity in the stomata cavities is assumed to have the saturation vapour pressure at the given leaf temperature [eq. (B3)].

2.4. Boundary and initial conditions

The system of model equations is closed and can be used for calculation of the meso-meteorological regime inside the vegetation as well as above it. Taking into account variations in the PBL height, which seldom exceeds 2500 m, we therefore assumed the top border of our model to be about 3000 m height (z_{00}). This height generally corresponds to an atmospheric pressure of about 700 hPa, for which basic meteorological parameters are generally provided from synoptic maps. The boundary conditions on the top and bottom are described in detail in Appendix C [eqs. (C1)–(C12)]. Here we limit our discussion to problems associated with boundary conditions at the lateral borders and to the initial conditions for the equations of our model.

The lateral boundary conditions necessary for a fine grid model are obtained from a background model. In order to obtain them for the area of interest we have used the method of zooming. For the lateral boundary conditions for u, v, T, q, C from the background model being realized for a coarse grid we have used:

$$\begin{aligned} &u = f_1(y,z,t), \quad v = f_2(y,z,t), \quad T = f_3(y,z,t), \\ &q = f_4(y,z,t), \quad C = f_5(y,z,t) \quad \text{for} \quad x = \pm X, \\ &u = f_1(x,z,t), \quad v = f_2(x,z,t), \quad T = f_3(x,z,t), \\ &q = f_4(x,z,t), \quad C = f_5(x,z,t) \quad \text{for} \quad y = \pm Y, \end{aligned} \tag{17}$$

where the functions f_j, $j = 1, 5$ are given by measurements or defined from the large-scale model (Penenko and Aloyan, 1985; Kunz and Moussiopoulos, 1997) and $x = \pm X$ and $y = \pm Y$ are the limits of the integrating domain over x and y directions respectively. In the present version we apply the method of one-sided interaction. This method considers the effects of processes described for surrounding areas on the coarser grid on the processes modelled to occur on the finer grid within our model's domain. The reverse effect is neglected. It is for this reason that variables are defined only on gridpoints where an external influence occurs (windward points).

The initial conditions at $t = 0$ can be obtained from observational data. However, detailed observed information on all meteorological parameters is difficult to obtain for a domain of non-uniform vegetation types. Thus, the following initial conditions have been used in most of our numerical experiments:

$$w(z) = 0, \quad u(z) = u_g, \quad v(z) = v_g, \quad e(z) = 0,$$

$$l(z) = 0.40 z_0, \quad C(z) = C(z_{00}), \quad q(z) = q(z_{00}),$$

$$T(z) = T(z_{00}) + \gamma_a (z_{00} - z) \tag{18}$$

2.5. Computational domain and numerical aspects

Figure 1 shows the general structure of the model, illustrating the link between the background and fine numerical grids and the characteristic dimensions used within each grid. Also shown are the main boundary condition variables and representative vertical profiles of the wind velocity components, air temperature, specific humidity and CO_2 concentration typically obtained from the model calculations. Using the data on the turbulence coefficient profile obtained during calculations, it is possible to deduce the fluxes of all necessary variables. The relationships between separate processes described in each grid cell and characteristic horizontal grid cell size are shown in Fig. 2; in this case specifically for a grid box within the vegetative layer. In the simulations described here, the number of gridpoints on the horizontal plane has been allowed to vary according to the particular task required, but the vertical irregular grid (with a minimal step at the surface 0.17 m and a maximum at the upper boundary of 200 m) remains constant, with 75 levels being present. The lowest 35 m of the model are divided into 42 computational levels which provide the necessary accuracy for a detailed description of the canopy structure and the processes occurring within it.

The system of non-linear differential equations of turbulent flow inside and above the non-uniform vegetation canopy is solved using a finite-difference method to split the equations into a set of algebraic equations with tri-diagonal matrices, with forward differencing for the time terms and upstream differencing for advection terms. The equation for the scale of turbulence has been integrated by Runge–Kutta techniques.

Although the atmospheric processes within the model domain are clearly related to those occurring in adjacent areas, there are no special processes operating at the lateral borders that are not described by the model equations. Therefore, it is possible to calculate all dependent variables at the lateral boundaries using inward directed finite differences on x and y. This means that only function values at gridpoints of boundary and at internal gridpoints closest to the boundary are necessary for such calculation (Belov et al., 1989). We have used this approach during model verification and numerical experiments in order to reduce the computational requirements.

3. Description of the test sites

The model was evaluated with data sets from three experimental sites. These are described in some detail below.

3.1. Experimental site 1

We used a data set of surface measurements made in Scots Pine forest located on the western bank of the Yenesey River, about 35 km west of the village of Zotino in central Siberia, Russia (61°N, 90°E). The trees are 20 m tall and about 120 yr old. The projected leaf area index at the site was estimated to be 2. There are few understorey shrubs and the ground is covered by lichens and mosses which became progressively more desiccated and brittle during the observation period, since no significant rain fell during this time (O. Kolle, personal communication, 2001). The measurements were made during the time period from 24 June 1999 until 15 July 1999 at the meteorological tower equipped with an eddy-correlation system similar to that described for a nearby site by Llyod et al. (2002). Two of the sonic anemometers (one above the canopy at 25.7 m, the other at 1.4 m above the ground) were supplemented with fast-response LICOR 6262 infrared gas analyzers (IRGA) to measure eddy fluxes of water vapour and CO_2 at the two heights. Sonic virtual temperature was used to measure sensible heat fluxes. Concentrations of carbon dioxide and water

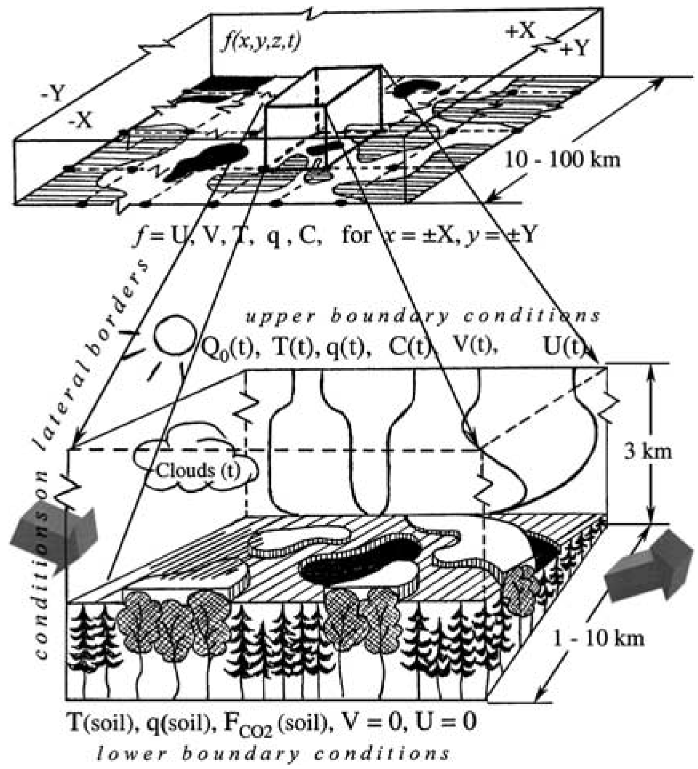

Fig. 1. The schematic representation of the model domain and boundary conditions as well as the coupling between background and fine grid models.

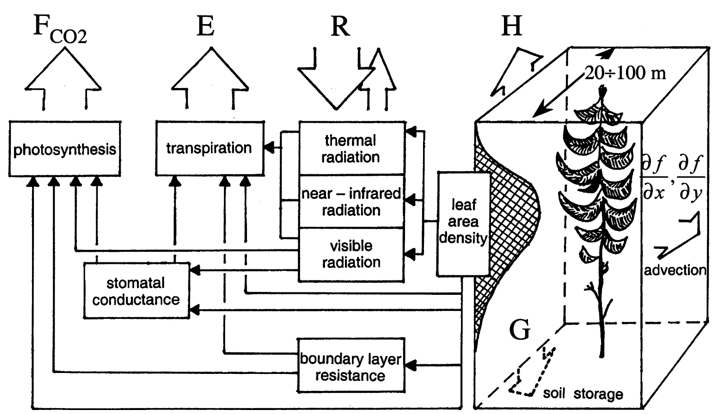

Fig. 2. The relationships between separate processes within a grid cell of the model.

vapour were measured in air sampled continuously at nine heights (six within canopy space, three above) and then passed sequentially via a gas-switch through the IRGA. Fine thermocouples were used to measure temperatures at the same heights as the air intakes (1.3, 6.1, 12.1, 13.9, 15.7, 17.5, 19.9, 22.9 and 26 m). Profiles of wind components were measured using five Gill sonic anemometers placed above and within the canopy at 1.4, 12.3, 16.2, 19.8 and 25.7 m (O. Kolle, personal communication, 2001).

In addition to these measurements, during the period from 28 June to 30 June at morning, noon and afternoon hours vertical profiles of air temperature and humidity and of CO_2 concentration were performed above the area of the experimental plot using an AN-2 aircraft. The airplane was instrumented with a simple system for the analysis of the concentrations of various gases in the atmosphere as well as for the measurement of ambient air temperature and pressure. Profiles of air temperature, water vapour and carbon dioxide concentrations were made within and above the CBL near the surface measurement site (See Lloyd et al., 2002; Styles et al., 2002).

3.2. Experimental site 2

The measurement site 2 was situated close to that of experimental site 1, also being located on the western bank of the Yenisey River about 40 km southwest of the village of Zotino. The vegetation of the plot is represented by a 215 yr-old stand of. *Pinus-sylvestris* . The 100 ha stand was established after fire that, by its recurrence, maintains a *P. sylvestris* monoculture. In the study stand, average tree height was 16 m, although some canopy emergent trees were as high as 22 m. Tree and lichen (*Cladonia* and *Cladina* spp.) understorey leaf area indices were 1.5 and 6.0, respectively, based on biomass measurements. From 8–25 July 1996 total forest and understorey latent heat flux densities were determined by the eddy covariance technique (Kelliher et al., 1998). Regional topography was gently undulating and the upwind forested fetch for measuring tower was adequate at around 1 km. On a larger scale, the region's vegetation is a mosaic of *P. sylvestris* forest and wetland. To estimate regional fluxes an airborne measurement technique was used. On 15 and 16 July 1996, a local Antonov-AN2 bi-plane was hired and three flights were undertaken on each day. Lloyd et al. (2001) present the aircraft data in more detail.

3.3. Experimental site 3

The third site is situated within the Central Biosphere Forest Reserve (CBFR) located about 300 km north-west of Moscow, Russia (56°27N, 32°55E) (Karpov, 1983; Varlagin and Vygodskaya, 1993). The main types of vegetation in this area are spruce (49%) and pine (12%) forests. Due to the numerous commercial thinning operations, forest fires and windbreaks over the last century, there are considerable areas of secondary forests present, these typically being dominated by birch, aspen and alder, which occupy 28%, 14% and 1% of CBFR area, respectively. As described in Section 4, the structure and spatial distribution of vegetation in CBFR is well studied and documented. Such information, along with a measurement data set of surface fluxes and meteorological variables (Naegler et al., 2002), is very valuable for model development and validation.

4. Results and discussion

Model validation and testing was undertaken in several stages. Initially the capability of the model to simulate the daily course of the main meteorological parameters of the atmospheric boundary layer was tested. For simplicity, the leaf aerodynamic resistance was assumed to be the same for all vegetation types in this model version, with c_d taken as 0.2. The integrated orientation of tree and understorey foliage was assumed as spherical and horizontal, respectively. The main parameters describing vegetation structure and properties, as well as that of the underlying soil are given in Table 1. The boundary conditions used in each experiment are described specifically for each case.

4.1. Experiments with the one-dimensional model version

Experimental site 1. To estimate the model's ability to simulate surface layer processes we used the measurement data from Scots Pine forest obtained in June 1999. This numerical experiment consisted of two components. In the first stage (analogous to a SVAT model) the calculations were made for a 26 m surface layer with the boundary conditions (BC) at the upper border corresponding to a real BC as measured at the top of the measurement tower at 26 m height. In the second stage, the calculations were carried out for the entire boundary layer based on boundary conditions at 3025 m height. To realise the first stage of the experiment the upper layers of the model were retrenched and the boundary conditions on unknown parameters were adapted accordingly. For the upper border of the domain ($h = 26$ m) we thus assumed a dependence of wind shear on friction velocity u_* and an impenetrability for turbulent energy flux as follows:

Table 1. *Stand structures and input parameters used in model simulations for three sites*

Site 1	Site 2	
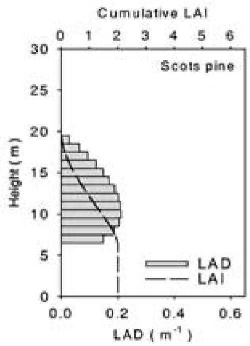	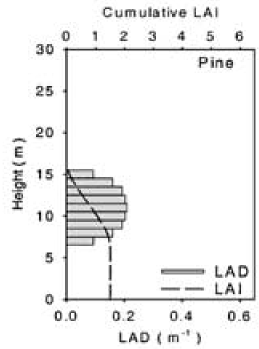	Sphagnum bog LAI = 4.0
λ = 700 (mol mol^{-1})	λ = 700 (mol mol^{-1})	λ = 1500 (mol mol^{-1})
Q_{50} = 43 (W m^{-2})	Q_{50} = 43 (W m^{-2})	Q_{50} = 43 (W m^{-2})
g_{st}^{max} = 0.0056 (m s^{-1})	g_{st}^{max} = 0.0056 (m s^{-1})	g_{st}^{max} = 0.0056 (m s^{-1})
g_{cut} = 0.000072 (m s^{-1})	g_{cut} = 0.000072 (m s^{-1})	g_{cut} = 0.000072 (m s^{-1})
$T_{min}, T_{opt}, T_{max}$ = 0, 18, 40 (°C)	$T_{min}, T_{opt}, T_{max}$ = 0, 18, 40 (°C)	$T_{min}, T_{opt}, T_{max}$ = 0, 18, 45 (°C)
d, d_f = 0.03 (m), 0.60	d, d_f = 0.03 (m), 0.50	d, d_f = 0.03 (m), 0.50
r_{PAR}, r_{NIR} = 0.09, 0.35	r_{PAR}, r_{NIR} = 0.09, 0.35	r_{PAR}, r_{NIR} = 0.09, 0.35
τ_{PAR}, τ_{NIR} = 0.06, 0.40	τ_{PAR}, τ_{NIR} = 0.06, 0.40	τ_{PAR}, τ_{NIR} = 0.06, 0.40
Loamy sand	**Sand**	**Water**
w_g, w_2 (m^3 m^{-3}) = 0.14, 0.14	w_g, w_2 (m^3 m^{-3}) = 0.05, 0.05	w_g, w_2 (m^3 m^{-3}) = 1.00, 1.00
$\alpha_{g,PAR}, \alpha_{g,NIR}$ = 0.10, 0.31–0.17w_g	$\alpha_{g,PAR}, \alpha_{g,NIR}$ = 0.10, 0.25	$\alpha_{g,PAR}, \alpha_{g,NIR}$ = 0.10, 0.15

Site 3		
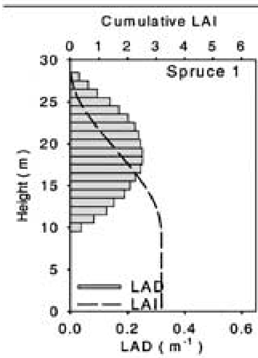	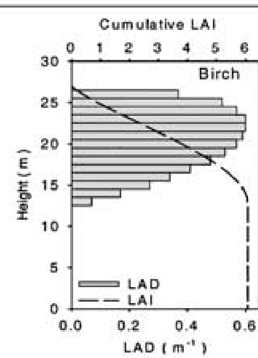	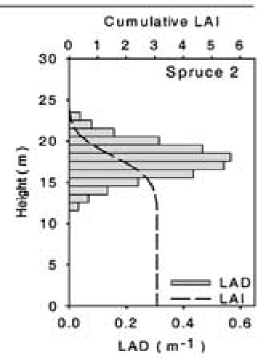
λ = 600 (mol mol^{-1})	λ = 800 (mol mol^{-1})	λ = 600 (mol mol^{-1})
Q_{50} = 20 (W m^{-2})	Q_{50} = 20 (W m^{-2})	Q_{50} = 20 (W m^{-2})
g_{st}^{max} = 0.0026 (m s^{-1})	g_{st}^{max} = 0.0046 (m s^{-1})	g_{st}^{max} = 0.0030 (m s^{-1})
g_{cut} = 0.000072 (m s^{-1})	g_{cut} = 0.00014 (m s^{-1})	g_{cut} = 0.000072 (m s^{-1})
$T_{min}, T_{opt}, T_{max}$ = 0, 17, 40 (°C)	$T_{min}, T_{opt}, T_{max}$ = 0, 18, 40 (°C)	$T_{min}, T_{opt}, T_{max}$ = 0, 19, 38 (°C)
d, d_f = 0.03 (m), 0.50	d, d_f = 0.05 (m), 0.50	d, d_f = 0.03 (m), 0.50
r_{PAR}, r_{NIR} = 0.09, 0.35	r_{PAR}, r_{NIR} = 0.09, 035	r_{PAR}, r_{NIR} = 0.09, 0.35
τ_{PAR}, τ_{NIR} = 0.06, 0.40	τ_{PAR}, τ_{NIR} = 0.06, 0.50	τ_{PAR}, τ_{NIR} = 0.06, 0.40
Loam	**Loam**	**Loam**
w_g, w_2 (m^3 m^{-3}) = 0.24, 0.24	w_g, w_2 (m^3 m^{-3}) = 0.24, 0.24	w_g, w_2 (m^3 m^{-3}) = 0.24, 0.24
$\alpha_{g,PAR}, \alpha_{g,NIR}$ = 0.10, 0.15	$\alpha_{g,PAR}, \alpha_{g,NIR}$ = 0.10, 0.15	$\alpha_{g,PAR}, \alpha_{g,NIR}$ = 0.10, 0.15

$$K_z \frac{\partial\sqrt{u^2+v^2+w^2}}{\partial z}\bigg|_{z=26\ \mathrm{m}} = u_*^2$$

$$\alpha_e K_z \frac{\partial e}{\partial z}\bigg|_{z=26\ \mathrm{m}} = 0. \tag{19}$$

Although there were observational data on the wind speed for a given height, the first condition in eq. (19) provided better agreement with measurements for both friction velocity and wind speed.

We used the half-hourly measurement data (with linear interpolation for each model step within that time interval) of downward short- and long-wave radiation fluxes, friction velocity, air temperature and humidity and of CO_2-concentration at the upper level corresponding to the height of sensors as input information for the SVAT model. At the lower border, the fit parameter a_{10} in the Lloyd–Taylor equation [eq. (C7), Appendix C] for soil respiration was set to 2.5 μmol m^{-2} s^{-1}. The time-dependent calculations were made from 00:00, 28 June to 24:00, 29 June with a numerical time step of 20 s. The temperature of the lowest soil layer was assumed constant and equal to 6 °C as observed at 0.5 m depth.

The model estimations of outgoing short- and long-wave radiation fluxes showed good agreement with measurement results, and the calculated net radiation above the plant canopy was close to that observed (Fig. 3A). The calculated values of vertical heat and water fluxes were also in good agreement with the measured data (Fig. 3B). The differences between the modelled and measured energy fluxes were most pronounced on the first day. There are two possible reasons: (1) the light rain (about 1 mm) which occurred in the morning of the first day was disregarded in the calculations here. This may have lead to

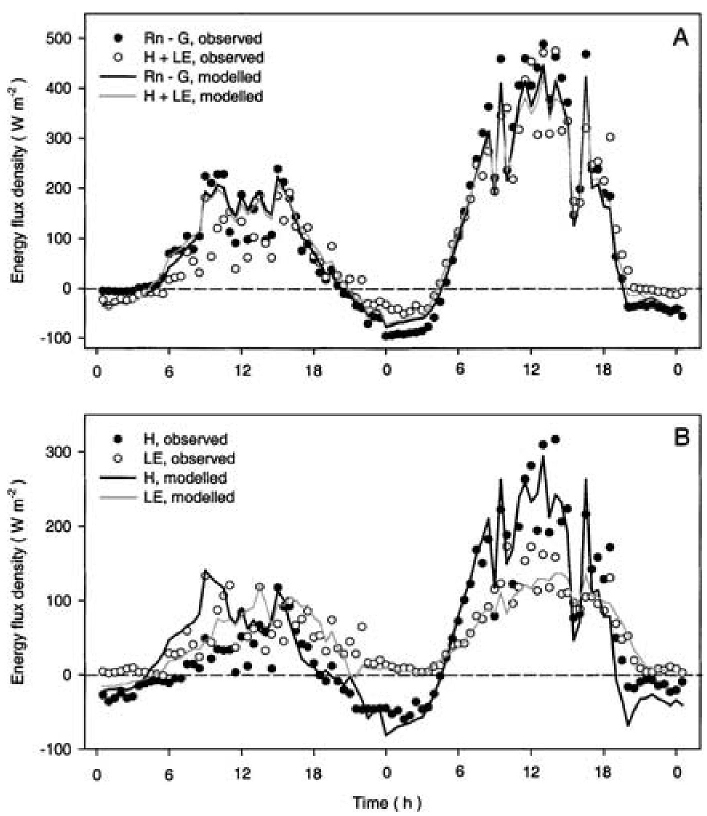

Fig. 3. Modelled and observed temporal course of the available energy, *Rn–G*, and the sum of sensible and latent heat fluxes, $H + LE$, (A) and separate sensible (H) and latent (LE) heat flux densities (B) above the forest at site 1 in Central Siberia during 28–29 June 1999.

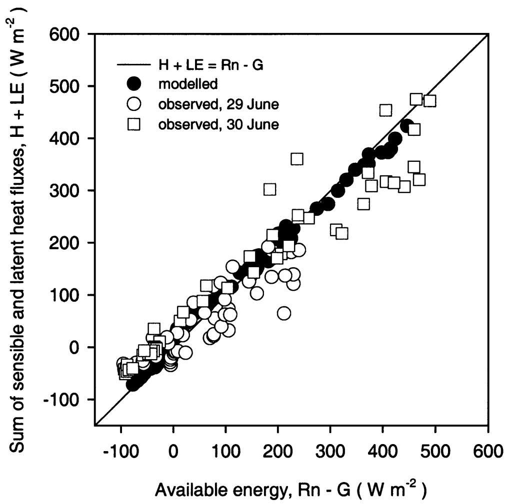

Fig. 4. The sum of sensible and latent heat fluxes, $H + LE$, versus available energy, $Rn - G$, for modelled and observed data above the forest at site 1 in Central Siberia during 28–29 June 1999. The 1:1 line is also shown.

underestimation of evaporation from the foliage surface; (2) some problems in the measurements can be seen when comparing the energy balance closure (Fig. 4). Our model implicitly closes the radiation balance, but a simple plot of $Rn - G$ versus $H + LE$ for the measurement data yielded a departure from the 1:1 line on the first day. By contrast, on the second day the experimental energy balance closure was much better (Fig. 4), and the model estimates of both H and LE were in much better agreement with the observed data (Fig. 3A).

Figure 5 shows the modelled and measured fluxes of carbon dioxide above the plant canopy for the same two days as Fig. 3. The model seems slightly to overestimate CO_2 fluxes around solar noon, especially for the second day. This may have been caused by the inertness of the chosen parameterization of photosynthetic response to the incoming solar radiation. On the other hand these deviations could be caused by problems with the parameterization of soil respiration or the fact that the model disregards stem respiration. Observations by Shibistova et al. (2002) in a nearby *P. sylvestris* stand showed that midday stem respiration rates can be of the order of 2 μmol m^{-2} s^{-1} in June/July during the period of intense cambial activity.

Measured and modelled CO_2 concentrations in the 26 m surface layer are presented in Fig. 6A and B, respectively. One can see that the model places the locations of main maxima and minima of CO_2 concentration within the canopy with sufficient accuracy. For the first day the model correctly calculated the first minimum of within CO_2 crown concentration between 9:00 and 10:00 related to the beginning of photosynthesis. The following minima at 13:00, 15:00, 18:00 and 22:00 correlated with peaks of incoming radiation are also described adequately. Some differences between measurements and model results observed for the second day were caused both by an increase of incoming radiation and by a higher friction velocity on this day. These features in turn resulted in an increase of errors in one-dimensional modelling. Nevertheless the model correctly reconstructed the main tendency of the CO_2 sink in the canopy. The minima around 9:00 and 12:00 are also correctly reconstructed;

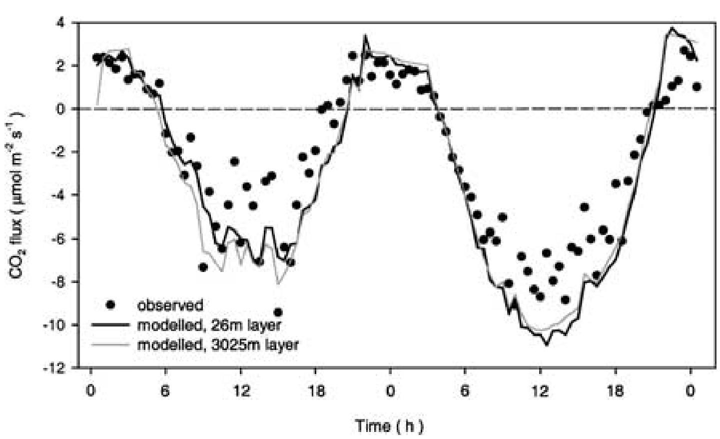

Fig. 5. Comparison between observed and modelled (with two different heights of upper boundary conditions) vertical fluxes of carbon dioxide above the forest at site 1 in Central Siberia during 28–29 June 1999.

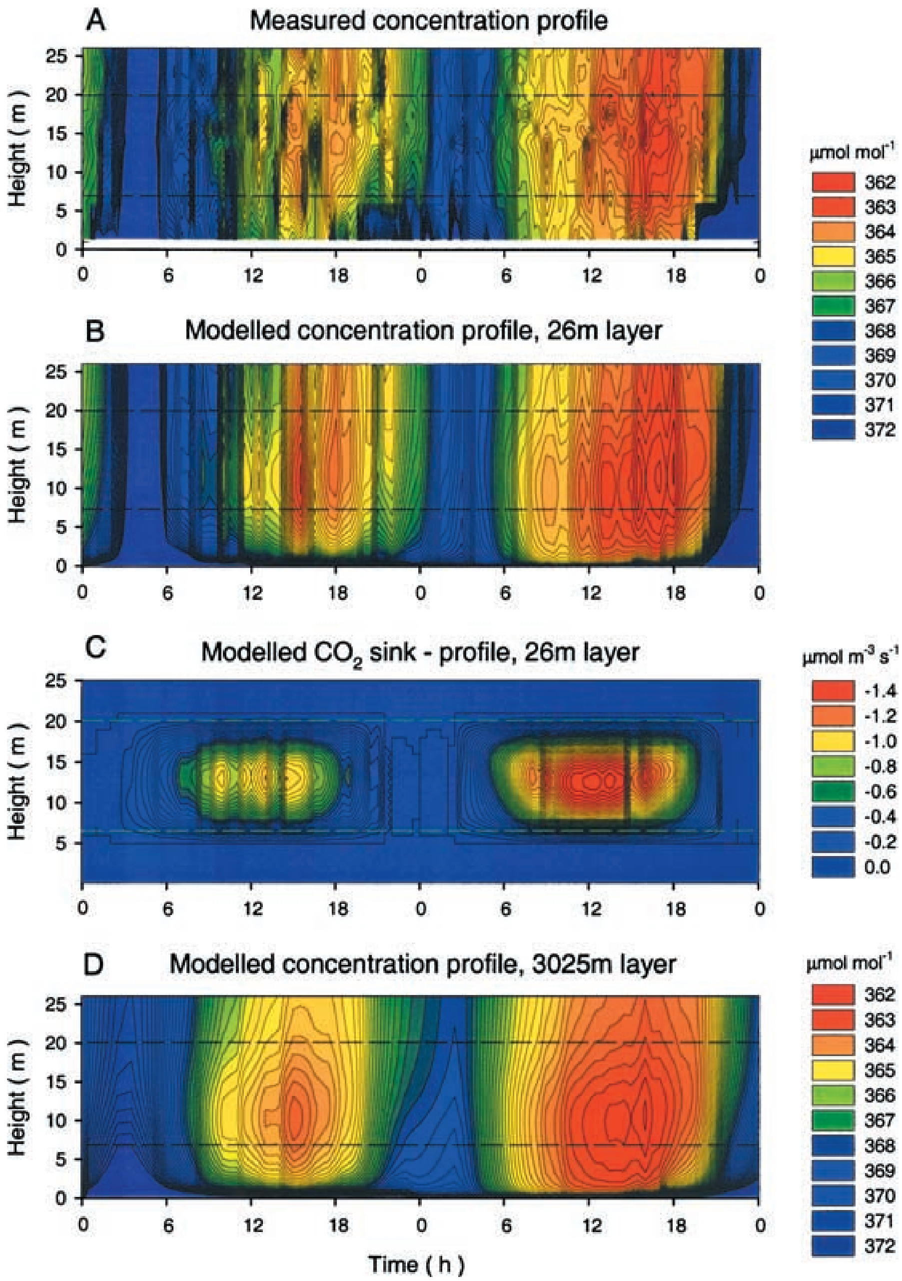

Fig. 6. Measured and modelled CO_2 concentrations. (A) Measured; (B) modelled with upper boundary conditions at a height of 26 m; (C) modelled with same upper boundary condition CO_2 sink profiles as a function of time within 26 m surface layer at site 1 in Central Siberia during 28–29 June 1999; (D) modelled with upper boundary conditions at a height of 3025 m for the same layer and time period. The dashed lines indicate bottom and upper borders of the needle area.

however, the minimum at 14:00 is somewhat underestimated when compared with the measurements. The difference fades out towards 17:00. This suggests that the LAD distribution assumed in the model needs a correction, or that the influence of advection during the daytime is considerable under the conditions of a sufficiently strong wind. The soil respiration is described adequately in general; however, the maxima of concentration occurred between 20:00, 29 June and 6:00, 30 June and are not reflected in the observed fluxes (Fig. 5) (our model gave a similar relation for the night fluxes as the measurements). This might also be explained by advective fluxes of CO_2 in the atmosphere, leading to increased CO_2 concentrations.

The comparisons suggest to us that the physical canopy model adequately describes the observed processes and, moreover, provides additional information. Such information is given in Fig. 6C showing the distribution of the CO_2 sink function for the same layer and time period. The vertical distribution of the sink function in the model allows us to determine the maximum of the CO_2 sink function in the canopy. It is interesting to note that there is inertia in the CO_2 concentration changes in the canopy. Figures 6B and 6C show that the maxima of the sink function and the minima of the carbon dioxide concentration are shifted relative to each other in time, especially during the first overcast day. The CO_2 concentration decreases gradually with increasing temperature; the CO_2 flux from the soil also increases. The inertia is not so noticeable during the second day because of the strong turbulent mixing.

To carry out the second component of the first experiment we used data from the National Centre for Environmental Predictions Reanalysis Project (NCEP) (Kalnay et al., 1986). The necessary data on wind speed, air temperature and humidity were interpolated from the numerical grid of this model onto the upper border (about 3000 m) of the model for 00:00, 06:00, 12:00 and 18:00 h Universal Standard Time, UST. Carbon dioxide concentrations at 3025 m were estimated using data from aircraft measurements, and were held constant (369 μmol mol^{-1}) for the two days of the experiment. Downward radiation fluxes were estimated from ground measurements. Because of the complicated pattern of incoming radiation fluxes we used the measured data to estimate the emissivity of the atmosphere first in order to estimate the cloudiness from eq. (A11) (Appendix A). Then the information on cloudiness was used to describe the pattern of incoming radiation.

The CO_2 flux modelled during this time period was very close to the one obtained from the surface layer model (Fig. 5). A smoothed course of geostrophic wind also provided a smooth course of modelled values of wind speed and friction velocity above the vegetation compared to the measurements (Fig. 7A). This in turn caused the smoothing of the modelled CO_2 concentration in (Fig. 6D) and above the plant canopy (Fig. 7B). As mentioned above the differences between the modelled and measured CO_2 concentrations during the night may have been caused by neglecting some sources of carbon dioxide such as advection.

Smoothing almost all modelled parameters above the canopy, including the air humidity, affected the humidity of the soil surface as well. Figure 7C shows the values of this parameter estimated during the measurements as well as from the models with an upper grid level of 26 and 3025 m. It should be noted that in spite of some differences, the method chosen for the description of soil moisture appears to be sufficiently adequate for our purposes.

Experimental site 2. For the first experiment information was obtainable on downward radiation fluxes and thus – on cloudiness. Without this information it would be impossible to describe the complicated meteorological conditions adequately. However, such detailed information is not always available. Sometimes, for example, there may only be information provided on the flux of available energy (Kelliher et al., 1998). In order to estimate the capability of our model to reconstruct the structure of an entire boundary layer with only limited data, a second numerical experiment was carried out.

A one-dimensional (1-D) model version was tested against measurements made in Siberia during the summer of 1996 (Section 3.2). The structural characteristics of the vegetation are given in Table 1. Two days with "clear-sky" conditions – (15 and 16 July) were chosen for the numerical experiment. The information on radiation fluxes above the vegetation was taken from the literature (Kelliher et al., 1998). Ground measurements showed that soil moisture was low, despite the fact that on average 55% of total water flux were contributed by the flux from the underlying surface covered by lichen. The six-hourly data from NCEP for this region was used as input information for the upper border of the boundary layer. The humidity data from NCEP did not, however, agree well with the data of aircraft measurements (Llyod et al., 2001). For this reason we assumed the mean value of two-days of aircraft measurements (1.6 mmol mol^{-1}) as the upper

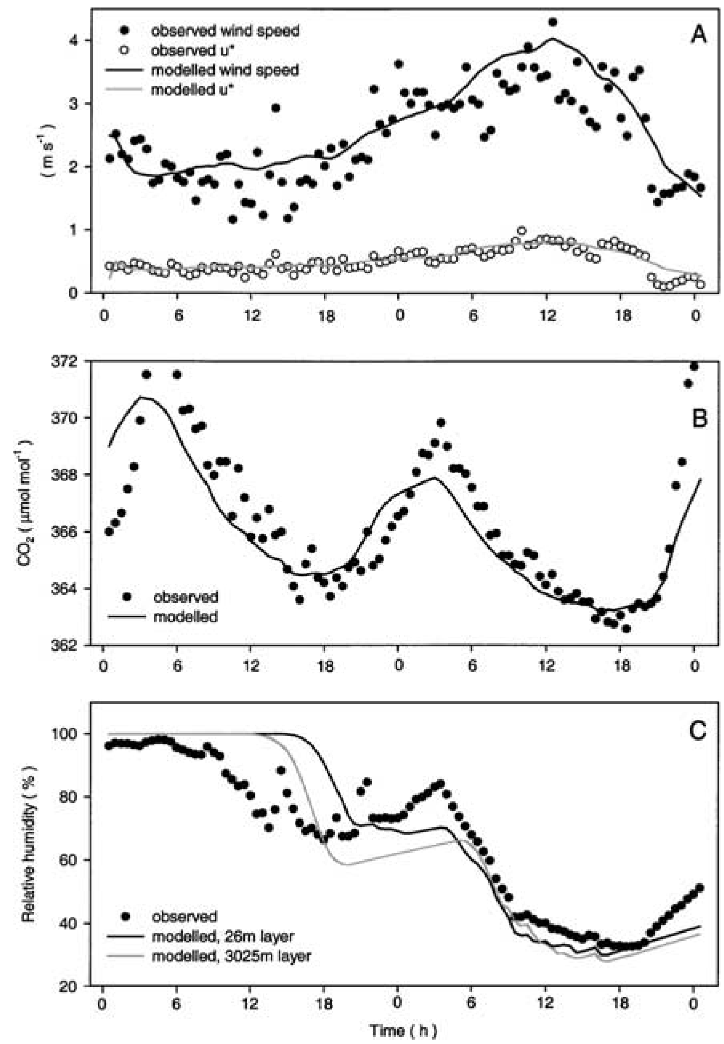

Fig. 7. Comparison between observed and modelled values of friction velocity and wind speed (A) as well as of CO_2 concentration (B) above the forest at site 1 in central Siberia during 28–29 June 1999. Upper boundary conditions set at the height of 3025 m. (C) Observed and modelled values of ground surface humidity for two different heights of upper boundary conditions.

boundary condition for air moisture. The carbon dioxide concentration at the upper border was also assumed as constant for two days and equal to 359 μmol mol^{-1} (Llyod et al., 2001). The coefficient a_{10} in the Lloyd–Taylor equation for soil respiration under forest was set to 1.0 μmol m^{-2} s^{-1}.

Llyod et al. (2001) showed that during two chosen days the descending air movement typical for anticyclonic weather was observed, with values varying from -2.1 to -5.0 mm s^{-1} at the 925 hPa level and from -5.5 to -11.0 mm s^{-1} at the 825 hPa level. To describe the vertical velocity in the model according to these conditions we chose a linear interpolation from 0.0 mm s^{-1} on the surface to -8.0 mm s^{-1} at the upper border of calculation layer. The calculations at 00.00, 15 July were initialized under the following conditions:

$$T = 10\,^{\circ}\mathrm{C}, \quad q = 8\,\mathrm{mmol\,mol^{-1}},$$

$$C = 350\,\mu\mathrm{mol\,mol^{-1}} \qquad \text{for} \quad z \leq 800\,\mathrm{m}$$

$$T = T(z_{00}) - 0.0063(z_{00} - z)\,^{\circ}\mathrm{C},$$

$$q = 1.6\,\mathrm{mmol\,mol^{-1}}, \quad C = 359\,\mu\mathrm{molmol^{-1}} \qquad \text{for} \quad z > 800\,\mathrm{m}$$

where z_{00} is the highest level of the model (z_{00} = 3025 m). These values are based on reasonable assumptions and on data from the first measurement flight of that day, which was made around 07.30 h.

In Fig. 8A measured and modelled net radiation as well as sensible and latent heat fluxes are presented for the second day of the experiment, 16 July. For an agreement between modelled and measured net radiation above the forest we assumed the atmospheric transparency as 0.7 and with cloud-cover fraction changing from 0.3 on the first day to 0.2 on the second one. In this experiment we ignored broken clouds, although some effects of these were clearly implied by the observational data. The comparisons between modelled and measured wind speed above the vegetation (Fig. 8B) suggest that the model adequately reconstructs the dynamic regime above the plant canopy.

Taking into account that the measured data of the boundary layer structure, against which our model was tested, were obtained above the vast area with a mosaic swamp distribution, the approximate area ratio of forest to bog being 5:1 (Llyod et al., 2001); the second-stage calculations were carried out with the same values of incoming short-wave radiation, but with an underlying surface in this case represented by bog vegetation (Table 1). The parameter a_{10} was taken as 3.0 μmol m^{-2} s^{-1}.

Figure 8A also shows that under the conditions of almost unchanged net radiation the modelled Bowen ratio above bog was changed for midday considerably (-0.7 instead of 3 above the forest) according to observed Bowen ratio (Valentini et al., 2000). This gives rise to significant differences in the modelled boundary layer development for the different surfaces. Figure 8B shows the observed and modelled values of air saturation deficit above the forest and at 2 m height above the bog. The overestimated model values of air saturation deficit above the forest (Fig. 8B) may be the result of one-dimensional modelling under the given conditions. For example, when the model surface is covered by bog completely, this deficit does not exceed 1.2 kPa.

It is clear that the energy exchange characteristics of a vegetative surface may exert significant feedback effects on its atmospheric environment. The variability range of boundary layer characteristics for two chosen underlying surfaces are clearly shown in Figs. 8C and 8D. We are not, therefore, implicitly trying to correctly reconstruct the observed boundary layer characteristics by means of the one-dimensional model employed here. Modelled and measured CO_2 concentrations may deviate due to the exclusion in the model of some vegetation types. There are six main vegetation types in the region, with tree stands of LAI varying between 1.5 and 2.5 m^2 m^{-2} (Schulze et al., 1999). When the underlying surface is assumed to consist of two vegetation types only, the preliminary conclusion could be drawn (Fig. 8E) that the boundary layer structure is influenced mainly by bog during night and morning hours and by the drier forest surface during the afternoon hours under the conditions of well developed turbulence.

In general it can be seen from Figs. 8C–E that the model slightly overestimates the height of influence of the underlying surface irrespective of whether that surface is considered to be "all forest" or "all bog". However, this estimation is less profound when the low Bowen ratio of bog surface is employed as the surface flux driver. This can be explained by an inability of the model to reconstruct the counterfluxes at the upper borders of the boundary layer as well as by possible errors in the assumed subsidence rates. However, the observed differences between measured and modelled data are, in fact, not so significant. The deviations for each surface type are presented in Fig. 9A. Here the temperature variations in the atmospheric boundary layer and in the soil of a forest-covered surface are shown for the two experiment days. Also the estimated boundary layer heights for both surface types, based on observational data and on data from a parametric model with a hypothetical surface, which is a mix of forest and bog areas in a relation of 5:1 (Llyod et al., 2001), are shown. Since the first experiment day might be considered as "adaptational", the height at pre-dawn is slightly overestimated as a consequence. However, for the second day the observed boundary layer height is within the range of model estimations for the two hypothetical uniform surfaces. It can be seen that boundary layer height is larger for the forest than for the bog, but that the growth of the boundary layer starts earlier above the bog. The tendency of boundary layer development in our model is in good agreement with modelled data of Llyod et al. (2001). However, the question is still open what ratio between different surfaces should be taken, to provide better agreement with measurements. Thus, one of the tasks for which the model could be applied is to estimate

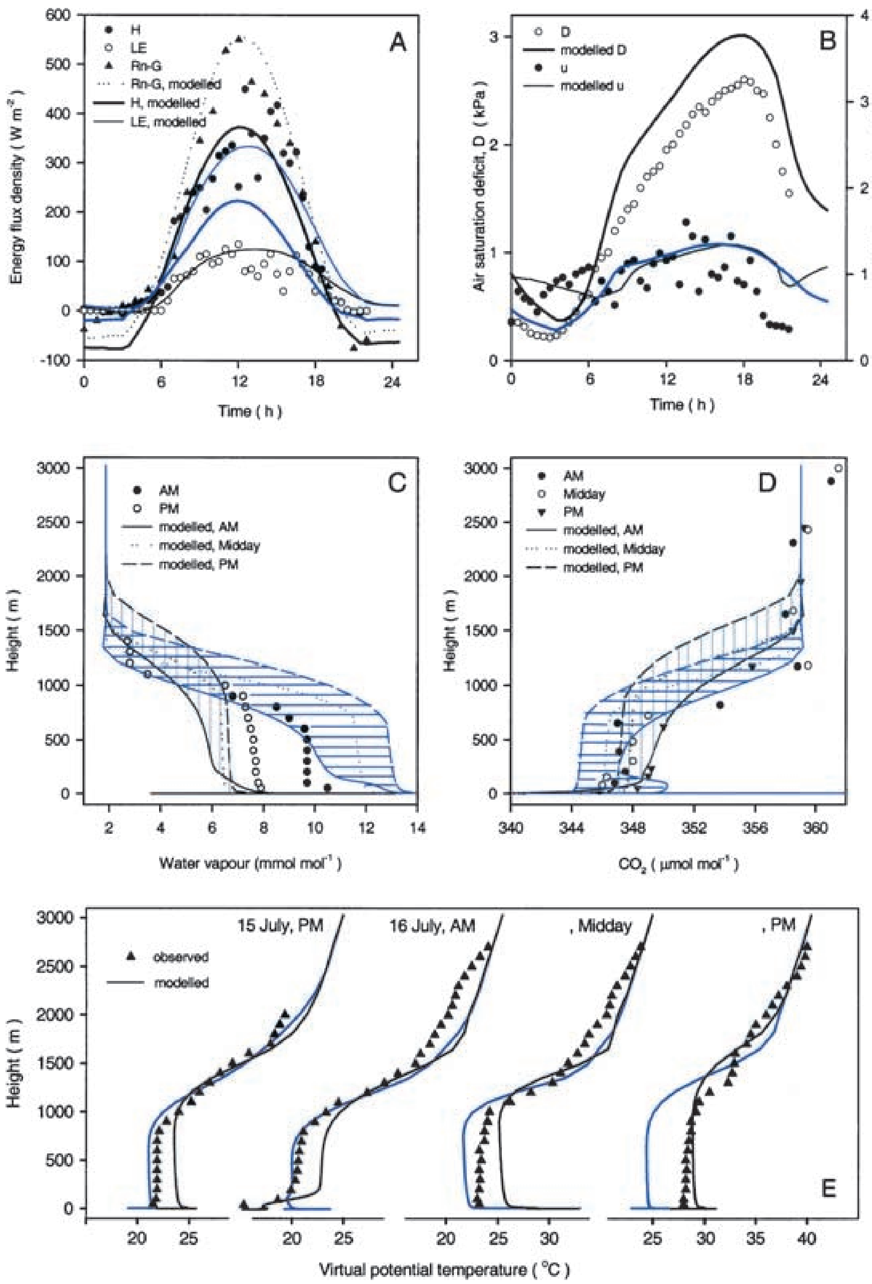

Fig. 8. Observed above-forest stand (symbols) and modelled above-forest (black lines) and bog (blue lines) surface meteorological variables and energy balance components at site 2 in central Siberia for 16 July 1996; (A) available energy, *Rn–G*, sensible heat, *H*, and latent heat, *LE*, flux densities; (B) air saturation deficit, *D*, and wind speed, *u*; (C) water vapour concentration; (D) carbon dioxide concentration; (E) virtual potential temperature during 15–16 July 1996 within PBL above the site 2 (AM around 06.00, Midday = 12.00 and PM = 18.00 local time). The dashed areas in panels C and D indicate variations of water vapour and CO_2 concentrations during the day, respectively.

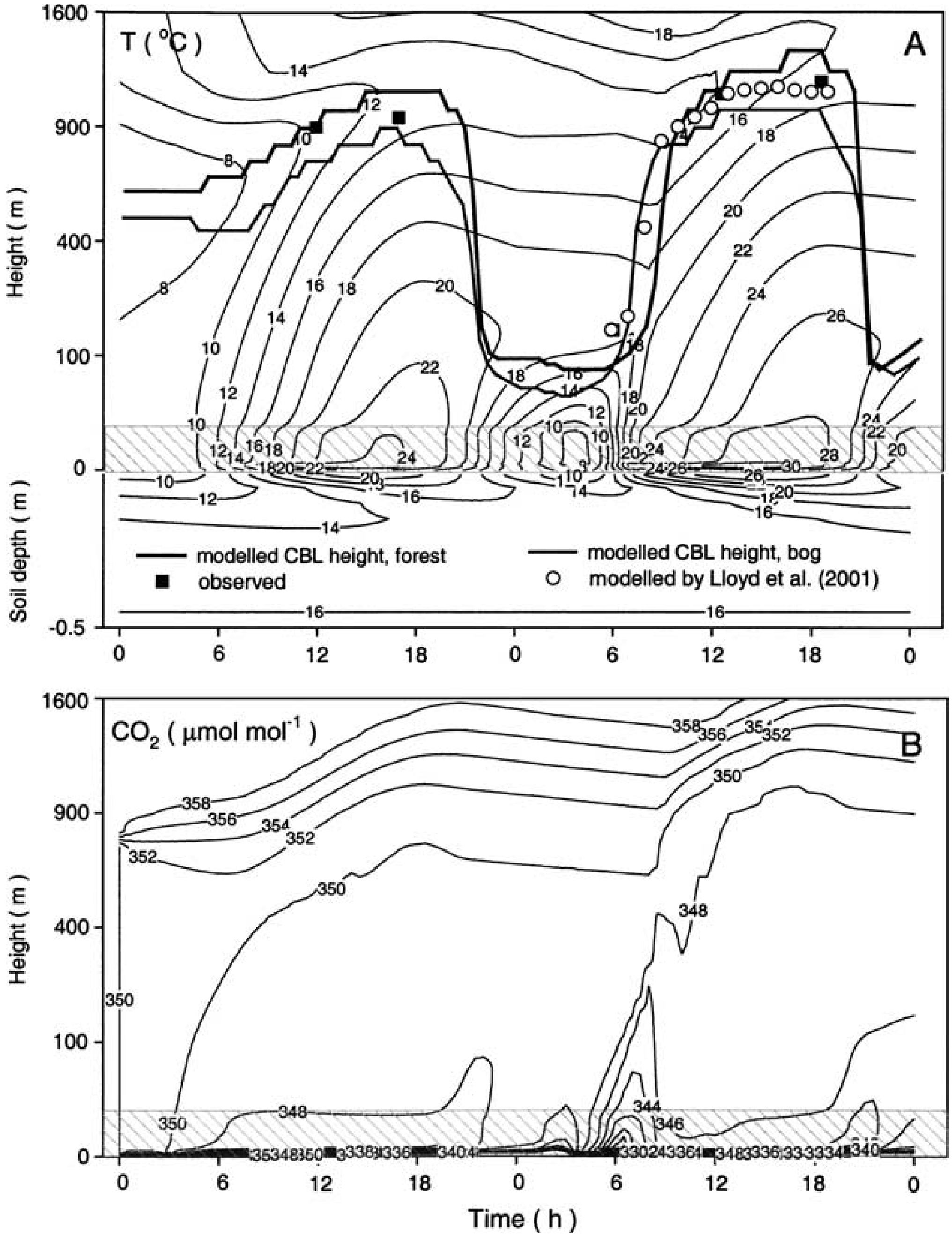

Fig. 9. Modelled variations of air and soil temperatures (A) and CO_2 concentration (B) above forest-covered surface at site 2 in central Siberia during 15–16 July 1996. The observed and modelled boundary layer heights for two experimental days as well as the boundary layer height estimated by the model of Lloyd et al. (2001) for 16 July 1996 are also shown (A) (for detail see text). The dashed areas in both panels indicate the canopy.

the contribution of each surface component in the formation of the boundary layer structure as a whole. However, in the present article we will not discuss this problem in detail, as it requires more specialized investigations and additional experiments.

The variations of the CO_2 concentration in the PBL above the forest during two days are presented in Fig. 9B. It could be noted that despite deviations from the observed vertical profiles of CO_2 mentioned above (Fig. 8D), the general tendency of the carbon dioxide transport within the PBL seems to be described adequately. During the first morning hours (day 2) the photosynthetic activity of the leaves in combination with weak turbulent exchange causes strong vertical difference in CO_2 concentration. Low CO_2 concentrations developed above the forest fade later due to a dramatic growth of the convective boundary layer. In daily course the concentration within the CBL remains constant because of intensive mixing. Towards the evening of 16 July as the turbulence attenuates, a small area of low concentration appears again but is quickly filled up by CO_2emitted by the soil. Limited nocturnal build-up of CO_2 occurs, however, due to the short night length and the low overall soil CO_2 efflux rates (Shibistova et al., 2002).

The above results illustrate the ability of the model to reconstruct the characteristics of PBL within and above the vegetation canopy, assuming homogeneity of the underlying surface. At the same time the numerical runs with the one-dimensional model indicate that an accurate description of the structure of the PBL requires detailed data on preceding conditions as well as on cloudiness, for improved description of incoming radiation fluxes. However, as a whole this lack of information does not affect the relationships between the different types of underlying surfaces, and thus the model could be used to estimate these relations and regularities. In the following experiments to further outline possibilities to apply the model, we do not consider complicated meteorological conditions. All calculations are made under the simplifying assumption that stable anticyclonic weather prevails.

4.2. *Experiments with the two- and three-dimensional model version*

In this part of the paper we focus on the variables that are directly related to the transport of passive tracers: in particular carbon dioxide. Our key emphasis here is the determination of effective flux "footprints" above a heterogeneous vegetation and the evaluation of environmental effects on CO_2 concentration and flux variability.

Experimental site 3. For numerical experiments with two- and three-dimensional versions of the model, the region around the monitoring station in CBFR near Moscow was chosen (Section 3.3). Figure 10 shows an aerial photograph of the test area (Fig. 10A) with the classification of the vegetation types (Fig. 10B) obtained from ground-based forest inventory data. Characteristics of these different vegetation types, used in the numerical experiments here, are given in Table 1. From these parameterizations, Figs. 10C and D show the spatial distribution of vegetation height and total LAI, respectively. For model runs, the horizontal resolution was set to 64 m for both the *x*- and *y*-coordinates of the model grid. A time step of 2 s was used to satisfy the CFL (Courant, Friedrichs and Levy) condition.

For the experiments with the 2-D model version, the vegetation distribution along the east–west transect $a-d$ (Fig. 10A) was taken. The spatial distribution of leaf area density (LAD) along this transect is shown in Fig. 11A. In these simulations the air temperature at the upper model border was taken as $0\,^{\circ}$C, the water vapour mole fraction was set to 2.4 mmol mol^{-1}, the velocity of the geosptrophic wind = 10 m s^{-1} and the CO_2 mole fraction was equal to 360 μmol mol^{-1}. An atmospheric transparency of 0.65 was assumed. Since the soil respiration rate estimated in CBFR by different methods had a high level of temporal and spatial variability (Naegler et al., 2002), we, for simplicity, assumed this value to be constant 4.5 μmol m^{-2} s^{-1}. The water content of the soil was taken as half of the full capacity for both layers. To reduce computing time, eq. (C2) (Appendix C) was used for calculations with the 1-D model version only. For the 2-D and 3-D modelling we used the parameterization of Nickerson and Smiley (1975) to describe the heat flux into the soil:

$$\left.\begin{aligned} G &= -0.19R_{\mathrm{gnet}} \quad \text{for} \quad R_{\mathrm{gnet}} < 0 \\ G &= -0.32R_{\mathrm{gnet}} \quad \text{for} \quad R_{\mathrm{gnet}} \geq 0 \end{aligned}\right\}. \tag{20}$$

The comparison of results of the numerical experiments performed with 1-D model for various G_l-parameterizations showed that the implementation of eq. (20) is realistic especially when reasonably dense vegetation is present above the ground surface.

Figure 11 also shows the results of the numerical experiment for the transect $a-d$ (Fig. 11A) for the surface layer at two points in time: just before

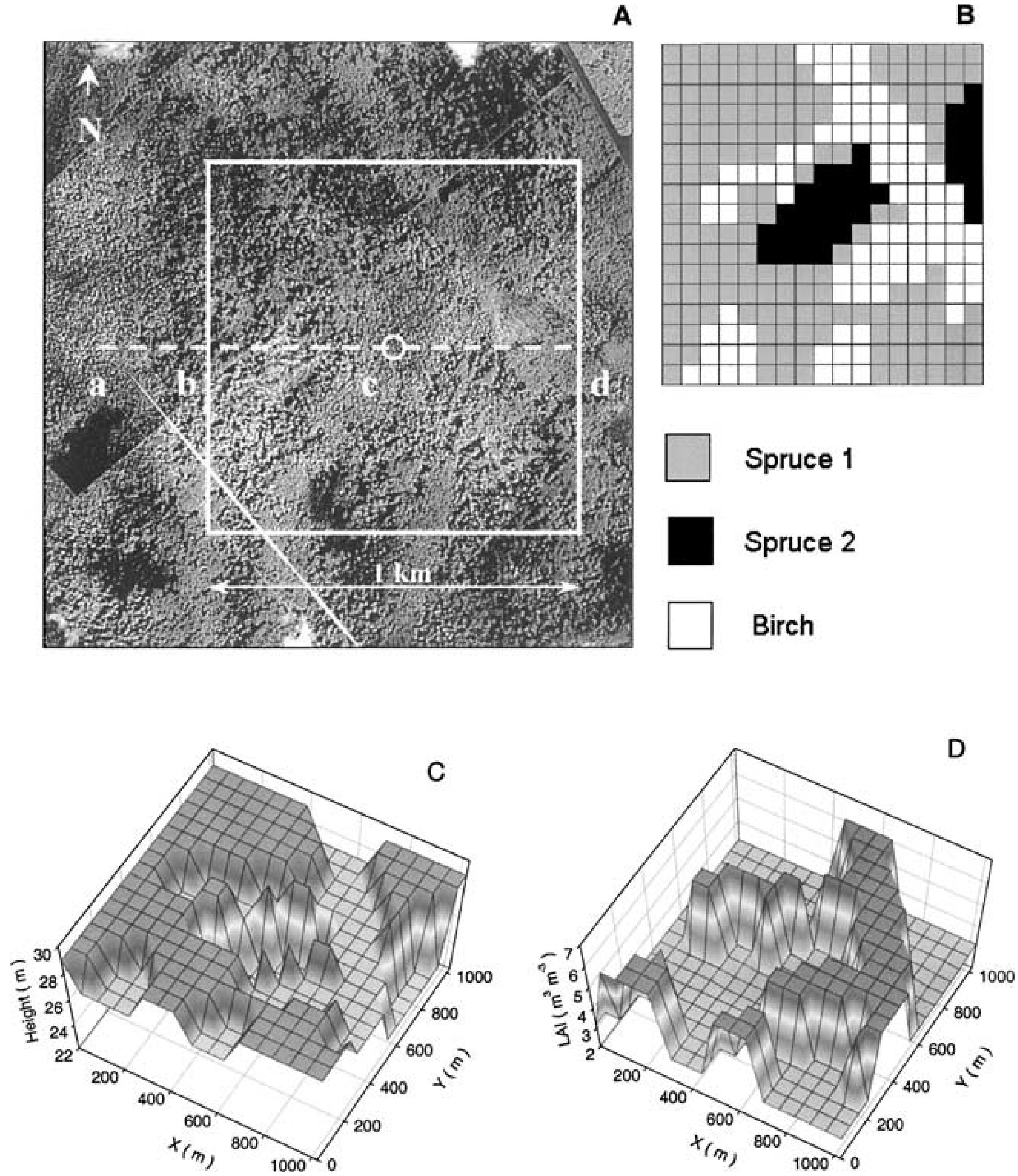

Fig. 10. The aircraft (aerial) photography of test area (A) and the model approximation of the vegetation type distribution (B), spatial distribution of vegetation height (C) and leaf area index (LAI) (D) of the area in west Russia (site 3). The tower location is indicated by the circle [point *c* (A)].

commencement of photosynthesis (3:00) and near the time of the maximum intensity of turbulence within the PBL (15:00). The local velocity scale

$$u_{\mathrm{L}} = \left[(K_z \partial u/\partial z)^2 + (K_z \partial v/\partial z)^2\right]^{0.25},$$

chosen here as a parameter representing the properties of the air flow above the surface (Fig. 11B), and the vertical turbulent flux of CO_2, as a measure of photosynthetic activity, (Fig. 11C) are also presented for both cases. The results show the surface to be relatively

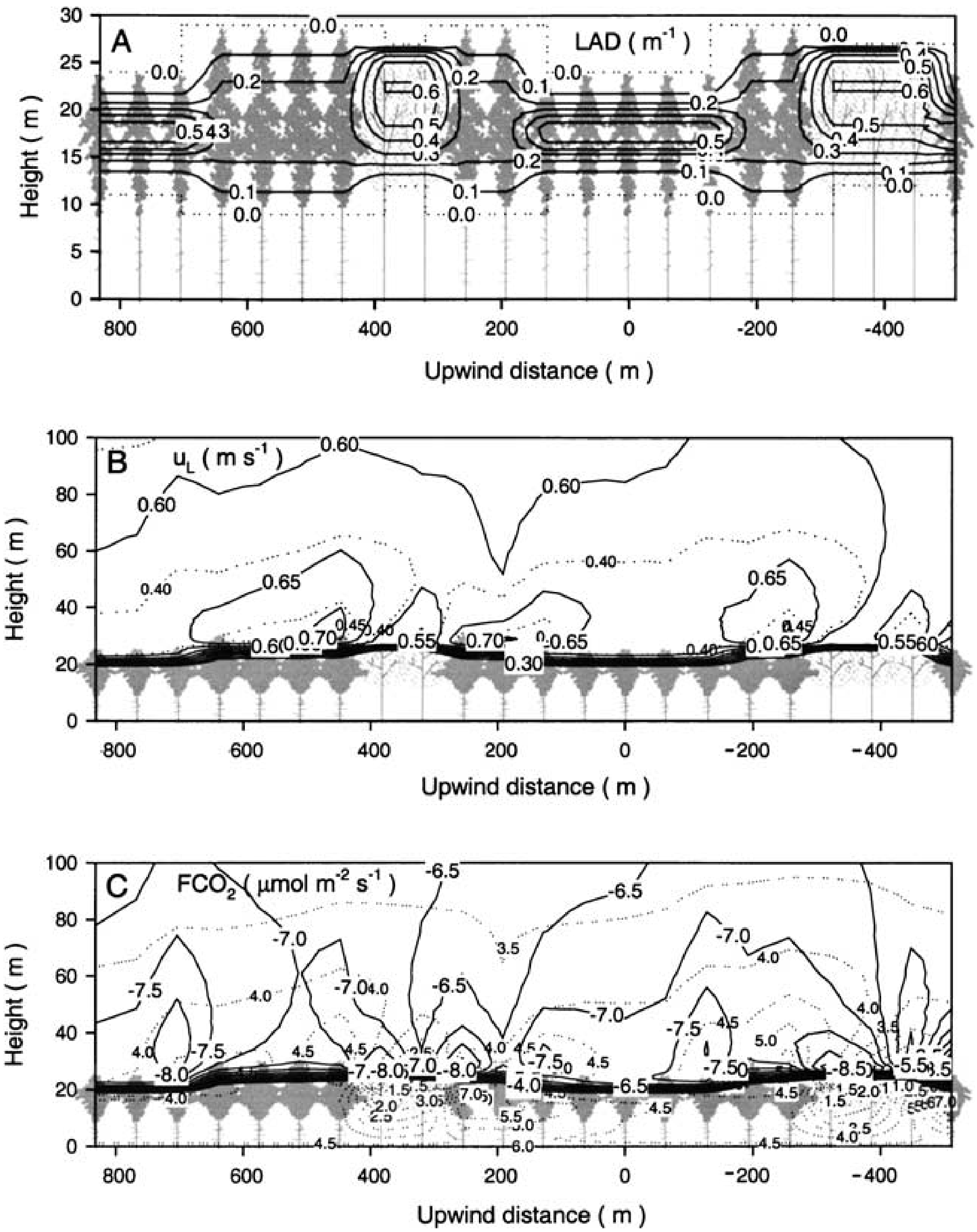

Fig. 11. The vegetation and its leaf area density (LAD) (m^{-1}) distributions along the east-west transect $a-d$ over the experimental site 3 (A). The results of the numerical experiment for the surface layer at the same transect for local velocity scale (B) and CO_2 fluxes (C) at two time points: before the start of photosynthesis 03:00 LT (dotted lines) and at the time of well developed boundary layer turbulence 15:00 LT (solid lines). Zero at x axis is the location of the tower.

homogenous in the sense of atmospheric dynamics, but with considerable temporal, vertical and horizontal differences being caused mainly by the variations in the photosynthetic activity of the vegetation.

In addition, we used the 2-D model version to evaluate the distance at which vertical CO_2 fluxes at the locations of eddy-correlation sensors on the measuring tower (point C in Fig. 10A) (34 m) and above it at the heights of 50 and 95 m are influenced. This is analogous to the so-called "footprint" question (Leclerc and Thurtell, 1990). The calculations carried out in this simulation are analogous to those results which are shown in Fig. 11C, but with the following modifications: (i) the spatial distribution of all meteorological parameters has been kept unchanged; (ii) the integral coefficients of the CO_2 exchange between the foliage as well as the soil and the surrounding air were set to zero everywhere except for the gridpoint along the x-axis, for which the influence on the measured tower fluxes we were interested to estimate. Moving through all grid points and knowing the distance of each point from the tower, it is possible to estimate the contribution of each grid point to the entire CO_2 flux at the site of the tower. After that the actual distribution of the tower footprint can be represented in its conventional form by taking the flux at the tower point as 1.

The results of such a calculation for different times are shown for the height of the measuring tower, for 50 m and for 95 m in Figs. 12A, B and C, respectively. The curves describing the footprints are similar to those obtained by analytic methods (Leclerc and Thurtell, 1990), and correctly reconstruct the movement of the footprint maximum when measurement height and time are changing. The position of the maximum influence on vertical fluxes shifts closer to the point of the flux measurements with decreasing measurement height and with increased turbulence in the afternoon. For example, during the afternoon hours the contribution of all CO_2 sources and sinks that are within a 800 m range upwind from the tower to the entire CO_2 flux measured at a height of 34 m is about 92% (Fig. 12A). This is only about 50% of the flux measured at a height of 95 m (Fig. 12C). Unlike the analytical footprint models usually applied,

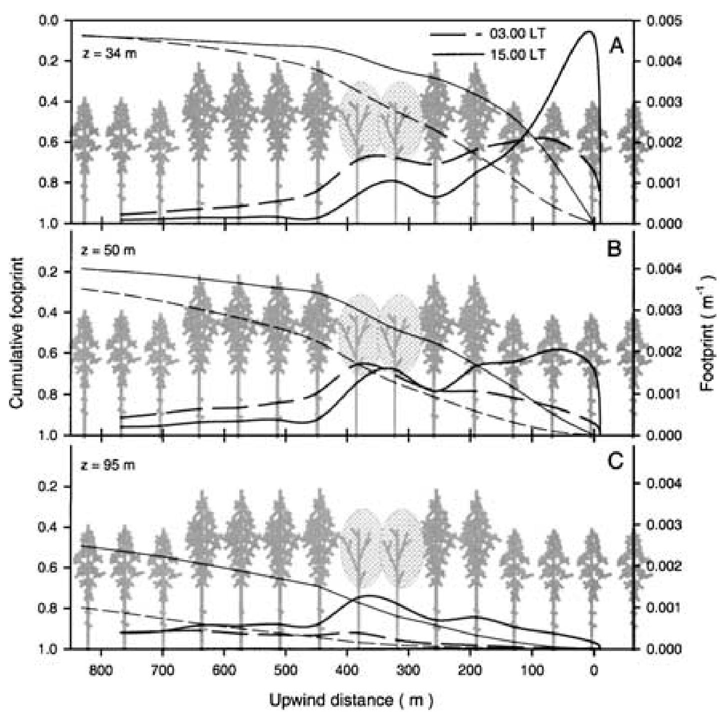

Fig. 12. CO_2 flux footprint estimation at 03.00 LT and 15.00 LT as a function of upwind distance for the three different levels above the measuring tower (see point c on Fig. 8A) (thick solid lines) as well as the cumulative normalized flux for same levels, obtained by integration of the footprint curves (thin solid lines). Zero at x axis is the location of the tower.

the method implemented in our model allows one to take into account the surface heterogeneity associated both with dynamic aspects (different resistance of different trees to airflow leads to a complex distribution of turbulent characteristics) and with variations in source and sink composition (different photosynthetic activity for different trees). That is why, even under such a rough model resolution (64 m is far from ideal for detailing the influence of horizontal heterogeneity) the footprint curve derived here is not smooth. Its oscillations at about 300 m upwind distance are the result of a non-uniform vegetation distribution (Rannic et al., 2000).

The results of 3-D modeling for the entire domain indicated in Fig. 10 are shown in Fig. 13. This figure illustrates the results obtained for 03:00 h and 15:00 h under conditions of a west–east surface wind direction (Figs. 13A and B, respectively) and for 15:00 h under conditions of north–south surface wind direction (Fig. 13C). It is clear that under the simulated conditions of constant illumination with the equal photosynthetic activity of different vegetation types and constant soil respiration, the CO_2 flux at the height of the sensor depends mainly on the peculiarities of the airflow. This dependence appears stronger during night-time (Fig. 13A). The upward airflow in front of the more aerodynamically dense birches leads to an intensification of the soil–atmosphere exchange and then to an increase of CO_2 concentration in higher layers (the blue area in Fig.13A). At the same time as the exchange weakens and CO_2 accumulates under the birch canopy, the CO_2 mixing ratio decreases above it (red areas in Fig. 13A).

Because of higher turbulent mixing such an aerodynamical contribution to the CO_2 flux at the sensor height is not significant during noon. It is appeared best under the conditions of west–east surface wind direction (red areas Fig. 13B).

The experiments with the 3-D model were carried out under the same upper and lower boundary conditions as with the 2-D model. The direction of gestrophic wind in one case was defined so that in the surface layer the wind was approaching the west–east direction. Calculation results of the local velocity scale and the vertical CO_2 flux obtained for transects $a-d$ (2-D version) and $b-d$ (3-D version) are compared in Fig. 14. It can be seen that the velocity scale and the vertical CO_2 fluxes generally agree very well, small deviations being possibly explained by transverse transport in the case of the 3-D model smoothing the fields of the wind speed and CO_2 mixing ratio.

The results of the 2-D and 3-D modelling indicate the strong influence of the windward lateral boundary conditions on modelled CO_2 concentration and fluxes. Even at a height of 34 m the 90% fetch distance is nearly 800 m (Fig. 12A). These experiments point out the limits for implementation of boundary conditions with inward directed finite differences. These conditions could be used to obtain preliminary characteristics only. For most accurate simulations it would be best to use the method of zooming, although this would require much higher computational costs.

Finally, the dependence of CO_2 flux variability on solar radiation is demonstrated in Fig. 15. In this numerical experiment we have introduced clouds into the model at several grid points (Fig. 15A). The clouds were kept constant for a 20 min period between 15:00 and 15:20. The spatial distribution of the vertical CO_2 fluxes at the beginning of the cloudy period is set at the height of the measuring instrument (34 m), as is shown for the previous simulations in Figs. 13B and C. As a consequence of the relative decline in incoming solar radiation because of the clouds (Fig. 15B), the CO_2 flux is modelled to increase in some regions by more than 5% (Figs. 15C and D).

This increase is a consequence of three factors: (i) the relative decrease in incoming PAR caused by cloud cover is less than the decrease in global radiation. This is because of a relative increase in the diffuse PAR fraction as a consequence of scattering by clouds; (ii) the diffuse radiation penetrates deeper into the vegetation canopy than does the direct radiation. This results in lower vegetation layers getting more PAR under cloudy sky conditions than in full sunlight: and (iii) there is a decrease in leaf temperatures, especially for the sunlit portion of the canopy. Under conditions of a relatively high temperature of the ambient air (about 28 °C in this experiment) and an associated high canopy-to-air vapour pressure difference, the lowering of leaf temperatures results in an increase in stomatal conductance and by virtue of this, in canopy photosynthetic rates.

It should be noted that CO_2 fluxes change most downwind relative to the location of the clouds and, for both wind directions, simulated areas of maximal change are within the region where the combination of different vegetation types is shaded by clouds (upper right quarter of Figs. 15C and D). This suggests that along with the physiological factors mentioned above, changes in the turbulent regime under conditions of broken clouds also change CO_2 fluxes. The

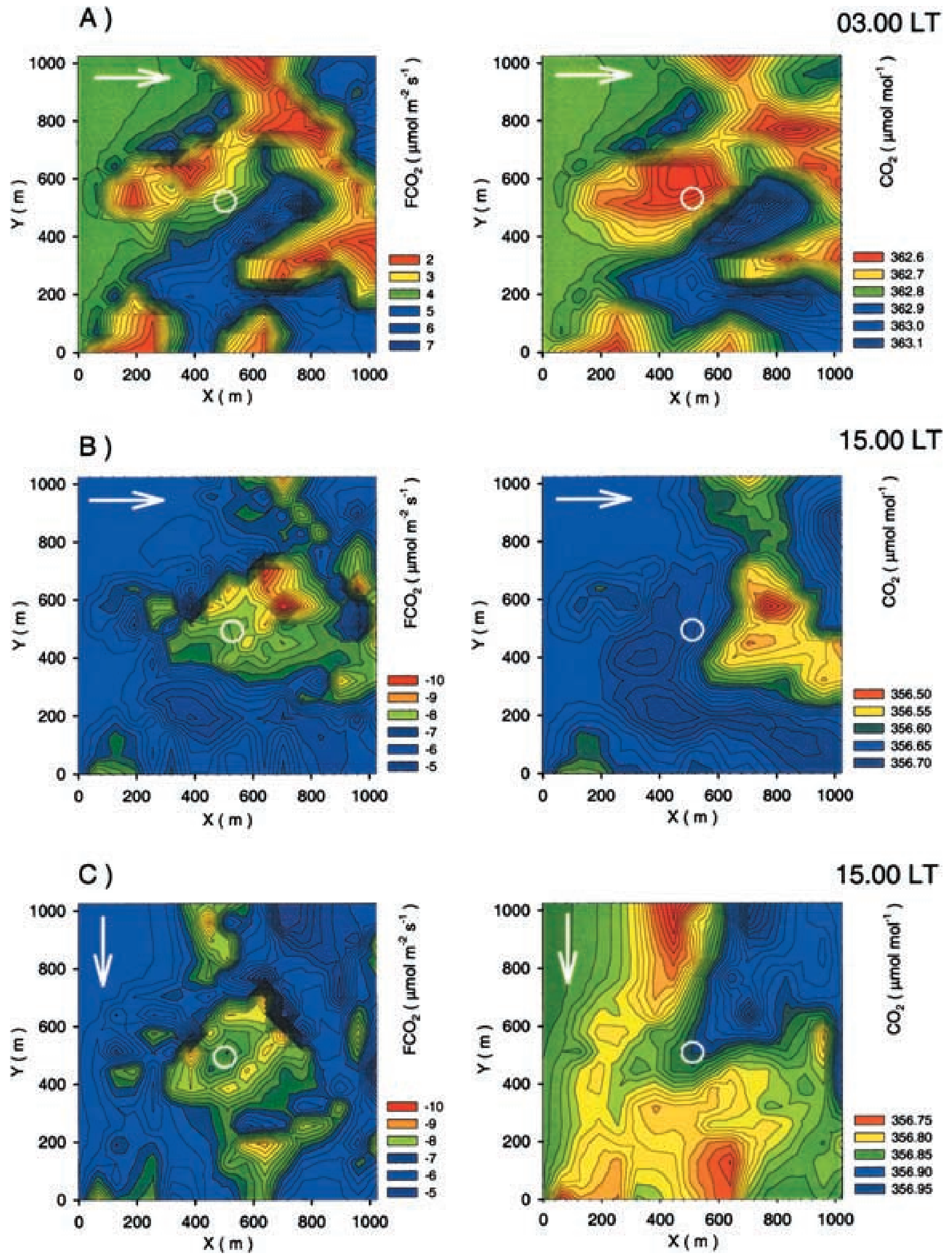

Fig. 13. The modelled carbon dioxide fluxes and CO_2 concentration distributions near the measuring tower for the west–east surface wind direction at two instances, 03.00 LT (A) and 15.00 LT (B), and for the north–south surface wind direction at 15.00 LT (C). The results are shown for the horizontal plane at the height of the measuring tower (34 m). Arrows indicate the wind directions above the canopy. The tower location is indicated by the circle.

answer to the question of what is the influence of each particular factor requires more detailed investigation and is outside the scope of this present article. However, it should be noted that the CO_2 flux around the tower was also changed in the simulation, even though the radiation field, there, remained unaffected. In

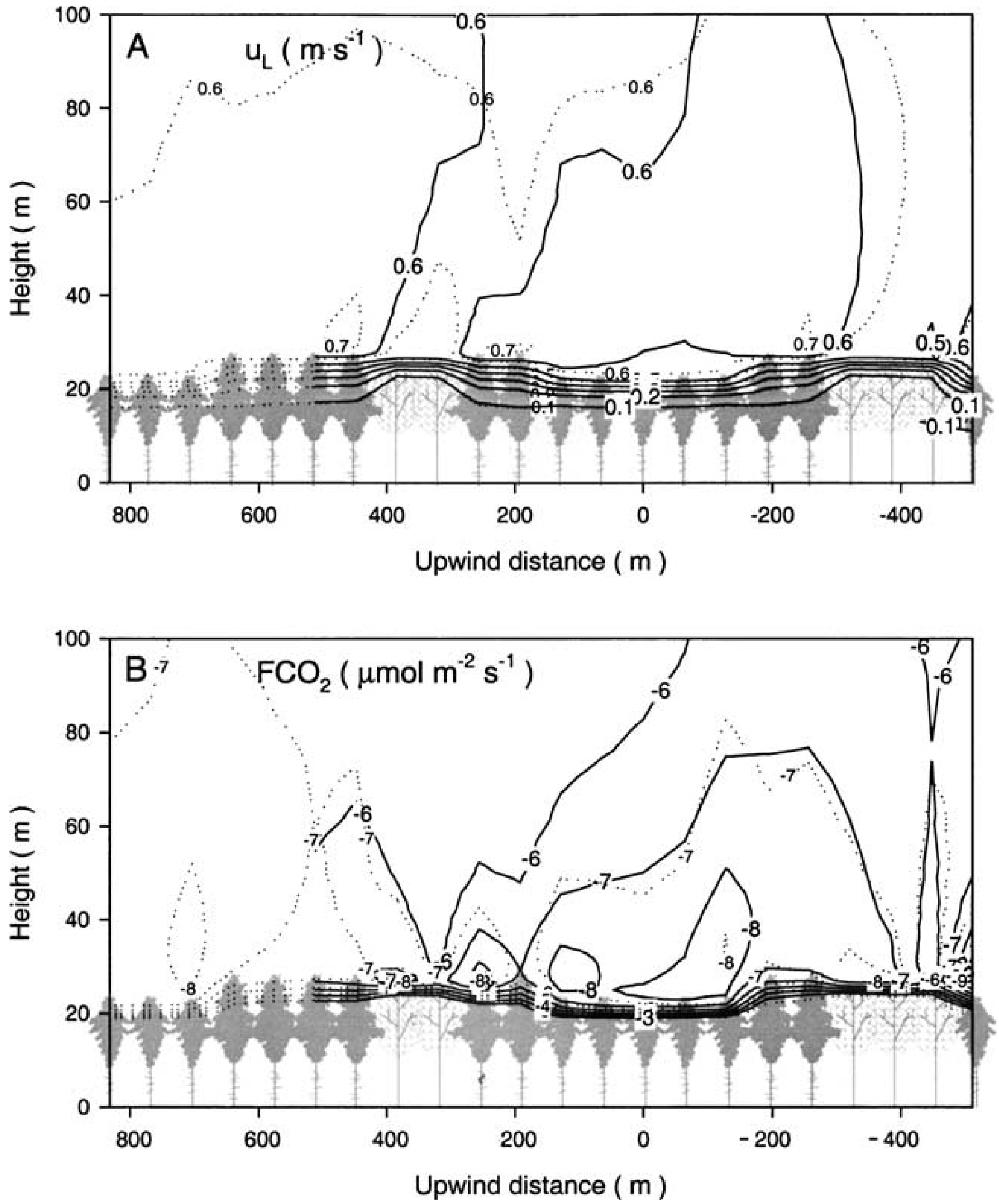

Fig. 14. The smoothing effect of the 3-D modelling against 2-D modelling. Comparison of modelled results for the local velocity scale (A) and the vertical CO_2 flux (B) obtained for transects $a-d$ (2-D version) (dotted lines) and $b-d$ (3-D version) (solid lines) at 15.00 LT.

reality such an underestimation of the broken clouds effect could lead to some errors when interpreting the factors determining the values of measured CO_2 fluxes.

5. Conclusions

In this paper we have introduced a three-dimensional model, SCADIS (scalar distribution),

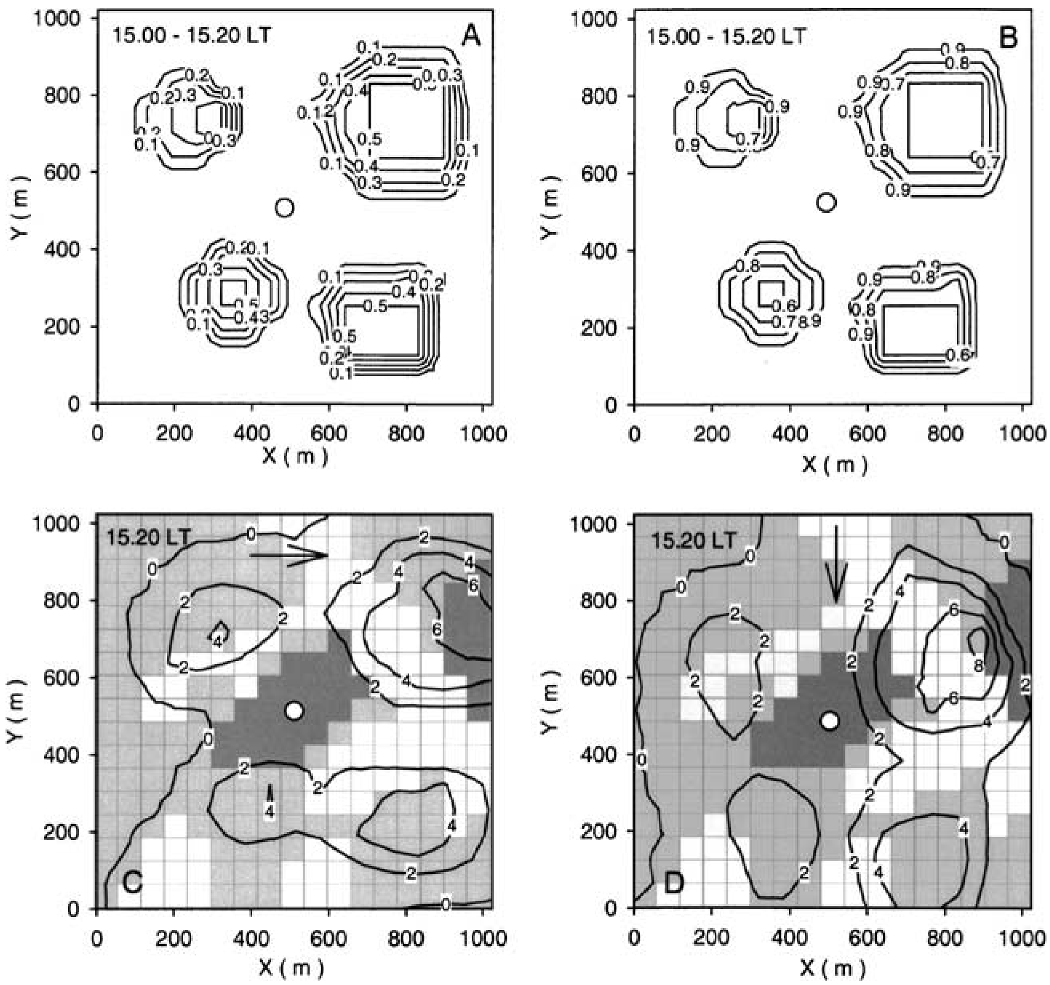

Fig. 15. The dependence of CO_2 flux variability on the radiation conditions. The modelled distribution of broken clouds (cloud-cover fraction) (A) and the relative decrease of incoming solar radiation (B) during a cloudy period (15.00–15.20 LT) as well as the changes in modelled CO_2 fluxes (%) just after this period (15.20 LT) for west–east (C) and north–south (D) surface wind directions. The changes in CO_2 fluxes are shown for the horizontal plane at the height of measuring tower (34 m). Arrows indicate the wind directions above the canopy. The tower location is indicated by the circle. The vegetation types distribution used in the model is also depicted in panels (C) and (D).

developed for simulation of processes in the canopy–planetary boundary layer. Despite of simplifications used to simulate natural processes, the first version of the model has demonstrated a reasonable agreement between modelled and observed data under different environmental conditions. Because of the simplicity of input parameters, the model only requires information on the LAD distribution and the synoptic meteorological data for initialization. An additional benefit is that it requires low computing time. Thus, it can be applied as a practical tool for many scientific tasks. A number of applications have been shown in the paper, such as (1) estimation of diurnal and spatial dynamics of CO_2 in the PBL in the presence of vegetation and under various synoptic conditions; (2) evaluation of environmental effects (aerodynamic and photosynthetic heterogeneity of vegetation) on CO_2 concentration as well as on CO_2 vertical fluxes at certain locations for various wind directions and for different times; (3) investigation of the influence of broken clouds on vegetation illumination and on resulting changes in the intensity of photosynthesis and spatial distribution of CO_2 concentrations.

Other applications of the model could be: (i) investigations of the spatial aggregation of energy fluxes across a heterogeneous landscape (the upscaling problem). (ii) investigations of the footprint for different tracer source distributions and for different weather conditions. A method analogous to the one used to calculate the upwind source influence on CO_2 flux at a certain point above the forest and shown here could also be applied to estimate footprints in a 3-D space. (iii) an investigation of the effect of spatial variations in illumination on the energy and CO_2 fluxes above a forest canopy. Equations of the leaf energy balance could be rewritten taking into account heat storage in order to consider the system's inertia. Defining the temporal and spatial distribution of cloud cover would make it possible to determine local patterns of heat, moisture and CO_2 fluxes and their common contribution to the flux from an entire experimental area or as measured at a fixed tower location. If at the same time the modelled illumination were to be kept constant above the point of measurement, it would be possible to evaluate the uncertainty of energy balance occurring there.

The solutions of such problems are of great interest to a wider scientific community. However, these investigations and their discussion were outside of the scope of the present study. We aim in the future to carry out these experiments as well as to improve our model using more complex parameterizations for some natural processes.

6. Acknowledgements

This research was partly EUROSIBERIAN CARBONFLUX project funded by the European Commission. We are sincerely thankful to Dr. O. Panferov of Institute of Bioclimatology, University of Göttingen, for the help in the development of the radiation module and for his support during the preparation of the manuscript. Special thanks to Olaf Kolle of the Max Planck Institute for Biogeochemistry, Jena, who provided us with data and useful information from the Scots Pine stand. We particularly acknowledge two anonymous reviewers for their useful remarks and comments.

Appendix A. Radiation parameterization

The natural changes in radiation external fluxes in the model are calculated using both empirical and astronomical formulas. Firstly we define the incoming radiation outside the atmosphere as

$$Q_0 = I_s \sin h_s, \tag{A1}$$

with

$$\sin h_s = \sin\varphi \sin\delta + \cos\varphi \cos\delta \cos t_s.$$

In these expressions I_s is the solar constant, φ is the geographic latitude, δ is the solar declination and t_s is the solar hour angle. δ can be calculated from (Tjernström, 1989), viz.

$$\delta = 0.4145 \sin\left(\frac{2\pi}{365.24} J\right),$$

where J is the calendar day with $J = 1$ at March 23. The total radiation above the plant (Q_h) is calculated taking in account the atmospheric transmittance (τ), the optical mass of atmosphere (m) and clouds as has been described by Campbell and Norman (1998) and Kondratev (1954):

$$Q_h = Q_0(0.3 + 0.7\tau^m)(1 - 0.8n_{\text{Low}} - 0.5n_{\text{Mid}} - c_{\text{High}} n_{\text{High}}), \tag{A2}$$

where n represents the cloud-cover fraction, and where subscripts Low, Mid, and High signify low, middle, and high clouds, respectively. The empirical coefficient c_{High} depends on zenith angle of the sun: $c_{\text{High}} = 0.2$ for $h_s > 20^\circ$ and $c_{\text{High}} = 0.4$ for $h_s \le 20^\circ$. m is given by Sivkov (1968) as:

$$m = 796\left(\sqrt{\sin^2 h_s + 0.002514} - \sin h_s\right).$$

Separating incident solar radiation into downward direct solar radiation flux I_h and downward diffuse sky radiation flux D_h on the upper boundary of vegetation (h) can be made by empirical formulas using information about the total radiation flux density; $Q_h = I_h + D_h$. We have used for this the estimation of the diffuse radiation proportion relative to the total incoming radiation outside the atmosphere (Q_0) as described in Spitters et al. (1986). The ratio between diffuse radiation (D_h) and total radiation (Q_h) is related to the ratio Q_h/Q_0 as shown in Table 2 (from Spitters et al., 1986).

The model estimates Q_0 and, as the values of incident (Q_h) are given, it is therefore possible to calculate the diffusive incoming radiation flux density (D_h) from Table 2. Then direct radiation (I_h) can be calculated as $I_h = Q_h - D_h$. However, the comparison of this method with others (Sivkov, 1968; Campbell and

Table 2. *Relationship between the ratio* D_h/Q_h *and the ratio* Q_h/Q_0 *for hourly radiation values (Spitters et al., 1986)*

$D_h/Q_h = 1$	For $Q_h/Q_0 < 0.22$
$D_h/Q_h = 1 - 6.4[(Q_h/Q_0) \times 0.22]^2$	For $0.22 < Q_h/Q_0 < 0.35$
$D_h/Q_h = 1.47 - 1.66Q_h/Q_0$	For $0.35 < Q_h/Q_0 < (1.47 - R)/1.66$
$D_h/Q_h = R$	For $(1.47 - R)/1.66 < Q_h/Q_0$
$R = 0.847 - 1.61 \sin h_s + 1.04 \sin^2 h_s$	

Norman, 1998) suggests that it may overestimate the proportion of diffuse radiation present under clear-sky conditions. To overcome this limitation, then, for all $Q_h/Q_0 \geq 0.22$ we correct the ratio D_h/Q_H by conversion factor $\alpha_D = (\frac{0.22}{Q_h/Q_0})^{0.37}$.

In this first stage of the development of our model we use the formulas and equations for radiation propagation within the canopy with spherically ($G_l = 0.5$) or horizontally ($G_l = \sin h_s$) oriented phytoelements, where h_s is current sun height and G_l is the integral function for leaf orientation (Ross, 1975). Therefore, for the description of radiation fluxes propagating in the canopy we assume that:

A.1. The penetration functions for the direct (η) and diffuse (μ) components of incident radiation

$$\eta(z) = \frac{I(z)}{I_h} = \exp\left(-\frac{G_l LAI(z)}{\sin h_s}\right), \tag{A3}$$

$$\mu(z) = \frac{D(z)}{D_h} = 2\int_0^{\pi/2} \exp\left(-\frac{G_l LAI(z)}{\cos\theta}\right)\cos\theta \sin\theta \, d\theta. \tag{A4}$$

Here LAI(z) is cumulative leaf area index (m^2 m^{-2}). The last equation has been written for the conditions of isotropic sky (Ross, 1975) with θ representing the solar zenith angle.

A.2. For complementary fluxes of scattered radiation due to the interaction of direct solar and diffuse sky radiation in the vegetation canopy in photosynthetic and near-infrared spectral ranges

In our model the fluxes of downward $F^{\downarrow}$ and upward $F^{\uparrow}$ scattered radiation are calculated using the equations (Ross and Nilson, 1967):

$$\left.\begin{aligned} \frac{dF_i^{\downarrow}}{dz} &= s(z)(1-\tau_i)F_i^{\downarrow}(z) - s(z)r_i F_i^{\uparrow}(z) - s(z)\tau_i[\eta(z)G_l I_H \sec\theta C_{S,i} + \mu(z)D_H C_{D,i}], \\ \frac{dF_i^{\uparrow}}{dz} &= -s(z)(1-\tau_i)F_i^{\uparrow}(z) + s(z)r_i F_i^{\downarrow}(z) + s(z)r_i[\eta(z)G_l I_H \sec\theta C_{S,i} + \mu(z)D_H C_{D,i}] \end{aligned}\right\} \tag{A5}$$

with the following top and bottom boundary conditions

$$\left.\begin{aligned} F_i^{\downarrow}(h) &= 0 \\ F_i^{\uparrow}(0) &= \alpha_{g,i}\left[C_{S,i} I_H \eta(0) + C_{D,i} D_H \mu(0) + F_i^{\downarrow}(0)\right] \end{aligned}\right\}. \tag{A6}$$

For the case of horizontally oriented leaves (Ross, 1975), the exact solution of eqs. (A5) is:

$$\left.\begin{aligned} F_i^{\downarrow}(z) &= Q_h \frac{a_1\left(e^{-a\mathrm{LAI}(z)} - e^{-\mathrm{LAI}(z)}\right) - a_2 e^{-2a\mathrm{LAI}}\left(e^{-a\mathrm{LAI}(z)} - e^{-\mathrm{LAI}(z)}\right)}{a_1 - a_2 e^{-2a\mathrm{LAI}}}, \\ F_i^{\uparrow}(z) &= Q_h \frac{b_1 e^{-a[2\mathrm{LAI} - \mathrm{LAI}(z)]} - b_2 e^{-a\mathrm{LAI}(z)}}{a_1 - a_2 e^{-2a\mathrm{LAI}}} \end{aligned}\right\} \tag{A7}$$

where the parameters a, a_1, a_2, b_1 and b_2 are defined as:

$$a = \sqrt{(1-\tau_i)^2 - r_i^2},\quad a_1 = \alpha_{\mathrm{g},i} - \frac{(1-\tau_i+a)}{r_i},$$

$$a_2 = \alpha_{\mathrm{g},i} - \frac{r_i}{(1-\tau_i+a)},$$

$$b_1 = 1 - \alpha_{\mathrm{g},i}\frac{(1-\tau_i+a)}{r_i},$$

$$b_2 = 1 - \alpha_{\mathrm{g},i}\frac{r_i}{(1-\tau_i+a)}.$$

In the above equation LAI is total leaf area density (m^2 m^{-2}), $\alpha_{\mathrm{g},i}$ is the soil albedo, F_i is the scattered radiation flux and r_i, τ_i are the leaf reflection and transmission coefficients for the i waveband of the radiation spectrum (i = NIR, PAR) and $C_{\mathrm{S},i}$ and $C_{\mathrm{D},i}$ are the PAR (0.42, 0.60) or NIR (0.58, 0.40) conversion factors for direct solar radiation and for diffuse radiation, respectively. The above formulas have been used in a number of models (e.g. Tuzet et al., 1993).

The analysis of numerical experiments has shown that the solution of the eqs. (A5) by means of a fourth-order accurate Runge–Kutta scheme is rather close to the solution of system (A7) for the case of horizontally oriented leaves. This holds true for trees with various LAI. For this reason we have only used one common algorithm based on eqs. (A5) to calculate scattered radiation fluxes for trees with different G_l.

A.3. For long-wave radiation

The downward $F_{\mathrm{LWR}}^{\downarrow}$ and upward $F_{\mathrm{LWR}}^{\uparrow}$ fluxes of thermal radiation are calculated using the following formulas (Ross, 1975; Dubov et al., 1978):

$$\left.\begin{aligned}\frac{\mathrm{d}F_{\mathrm{LWR}}^{\downarrow}}{\mathrm{d}z} &= s(z)\left(\delta_{\mathrm{LWR}}F_{\mathrm{LWR}}^{\downarrow}(z) - \delta_{\mathrm{LWR}}\sigma\left\{\eta(z)\left[T_l^{sn}(z)\right]^4 + [1-\eta(z)]\left[T_l^{sd}(z)\right]^4\right\}\right),\\ \frac{\mathrm{d}F_{\mathrm{LWR}}^{\uparrow}}{\mathrm{d}z} &= s(z)\left(-\delta_{\mathrm{LWR}}F_{\mathrm{LWR}}^{\uparrow}(z) + \delta_{\mathrm{LWR}}\sigma\left\{\eta(z)\left[T_l^{sn}(z)\right]^4 + [1-\eta(z)]\left[T_l^{sd}(z)\right]^4\right\}\right)\end{aligned}\right\}. \tag{A8}$$

Here σ is the Stefan–Boltzmann constant, and δ_{LWR} is the emissivity of a leaf. The boundary conditions for the solution of the equation set (A8) are

$$\left.\begin{aligned}F_{\mathrm{LWR}}^{\downarrow}(h) &= \delta_{\mathrm{a}}\sigma\,[T(h)]^4\\ F_{\mathrm{LWR}}^{\uparrow}(0) &= \delta_{\mathrm{g}}g\sigma(T_{\mathrm{g}})^4 + (1-\delta_{\mathrm{g}})F_{\mathrm{LWR}}^{\downarrow}(0)\end{aligned}\right\}, \tag{A9}$$

where δ_{g} is the ground surface emissivity and δ_{a} is defined as an apparent emissivity of the atmosphere. For clear-sky conditions, the emissivity δ_{a} depends on air temperature and humidity above the vegetation layer (Penenko and Aloyan, 1985)

$$\delta_{\mathrm{a}} = 0.526 + 0.065\sqrt{q(h)}\,[1250 + 4.575\,(T(h) - 273.15)]. \tag{A10}$$

The atmospheric emittance on cloudy days can be estimated by the simple relationship (Monteith and Unsworth, 1990)

$$\delta_{\mathrm{a}}(n) = (1-0.84n)\delta_{\mathrm{a}} + 0.84n \tag{A11}$$

where n is the fraction of the sky covered by cloud.

Appendix B. Energy balance equations for leaves

The set of unknown parameters includes two temperatures of phytoelements. Therefore, it is necessary to include equations for the leaf energy balance in our model. If heat storage and metabolic heat production are assumed to be negligible, the relevant equations for sunlit and shaded surfaces of the plants for each level are:

$$\begin{aligned}&s\chi_{\mathrm{PAR}}\left(IC_{\mathrm{S,PAR}} + DC_{\mathrm{D,PAR}} + F_{\mathrm{PAR}}^{\downarrow} + F_{\mathrm{PAR}}^{\uparrow}\right)\\ &\quad + s\chi_{\mathrm{NIR}}\left(IC_{\mathrm{S,NIR}} + DC_{\mathrm{D,NIR}} + F_{\mathrm{NIR}}^{\downarrow} + F_{\mathrm{NIR}}^{\uparrow}\right)\\ &\quad + s\delta_{\mathrm{LWR}}\left(F_{\mathrm{LWR}}^{\downarrow} + F_{\mathrm{LWR}}^{\uparrow}\right) = s_{\mathrm{H}}\rho_{\mathrm{a}}C_p g_{\mathrm{H}}^{sn}\left(T_l^{sn} - T\right)\\ &\quad + s_{\mathrm{V}}Lg_{\mathrm{V}}^{sn}\left(q_l^{sn} - q\right) + s_{\mathrm{H}}\delta_{\mathrm{LWR}}\left(\sigma T_l^{sn}\right)^4\end{aligned} \tag{B1}$$

$$s\chi_{\mathrm{PAR}}\left(DC_{\mathrm{D,PAR}}+F_{\mathrm{PAR}}^{\downarrow}+F_{\mathrm{PAR}}^{\uparrow}\right)$$

$$+s\chi_{\mathrm{NIR}}\left(DC_{\mathrm{D,NIR}}+F_{\mathrm{NIR}}^{\downarrow}+F_{\mathrm{NIR}}^{\uparrow}\right)$$

$$+s\delta_{\mathrm{LWR}}\left(F_{\mathrm{LWR}}^{\downarrow}+F_{\mathrm{LWR}}^{\uparrow}\right)=s_{\mathrm{H}}\rho_{\mathrm{a}}C_{p}g_{\mathrm{H}}^{sd}\left(T_{l}^{sd}-T\right)$$

$$+s_{\mathrm{V}}Lg_{\mathrm{V}}^{sd}\left(q_{l}^{sd}-q\right)+s_{\mathrm{H}}\delta_{\mathrm{LWR}}\left(\sigma T_{l}^{sd}\right)^{4} \qquad \text{(B2)}$$

where $\chi_i = (1 - \tau_i - r_i)$ is the leaf absorption coefficient for the i waveband of the radiation spectrum, and L is the latent heat of vaporization.

As it is commonly assumed, we suppose that the air humidity in in-leaf space (stomata cavities) is the saturation vapour pressure at the leaf temperature (Cowan, 1977). In this case for q_l^{sn} and q_l^{sd} (kg m^{-3}) the Magnus empirical formula is used:

$$q_l^{sn,sd} = q_{\mathrm{sat}}\left(T_l^{sn,sd}\right)$$

$$= \frac{1.3318375}{T_l^{sn,sd}}\exp\left(\frac{17.57\left(T_l^{sn,sd}-273.15\right)}{241.9+T_l^{sn,sd}-273.15}\right). \qquad \text{(B3)}$$

Appendix C. Top and bottom boundary conditions

C.1. Air temperature and humidity at the upper and lower boundaries

The ground surface energy balance equation

$$G + LE_{\mathrm{g}} + H_{\mathrm{g}} = R_{\mathrm{gnet}} \qquad \text{(C1)}$$

taken together with the basic equations for heat conduction in the soil

$$G = k_{\mathrm{s}}\left.\frac{\partial T_{\mathrm{s}}}{\partial z}\right|_{z=0} \qquad \text{(C2)}$$

and

$$\frac{\partial T_{\mathrm{s}}}{\partial t} = \frac{\partial}{\partial z}\kappa\frac{\partial T_{\mathrm{s}}}{\partial z} \qquad \text{(C3)}$$

is solved to obtain the ground surface temperature (T_{g}) that serves as lower boundary condition

$$T(0) = T_{\mathrm{g}}.$$

In eq. (C1) R_{gnet} is net short-wave and long-wave radiation flux at the ground surface and is calculated according to

$$R_{\mathrm{gnet}} = I_{\mathrm{H}}\eta(0) + D_{\mathrm{H}}\mu(0) + F_{\mathrm{PAR}}^{\downarrow}(0) - F_{\mathrm{PAR}}^{\uparrow}(0)$$

$$+ F_{\mathrm{NIR}}^{\downarrow}(0) - F_{\mathrm{NIR}}^{\uparrow}(0) + F_{\mathrm{LWR}}^{\downarrow}(0) - F_{\mathrm{LWR}}^{\uparrow}(0), \qquad \text{(C4)}$$

LE_{g} and H_{g} are latent and sensible heat fluxes at the ground surface, respectively (positive when directed upward), and G is the soil heat flux at the surface (denoted positive when directed into the soil). For eqs. (C2) and (C3) $k_{\mathrm{s}}, \kappa, T_{\mathrm{s}}(z)$ are the thermal conductivity, thermal diffusivity and temperature of the soil, respectively. The thermal conductivity of the soil is approximated by

$$k_{\mathrm{s}} = \max[418\exp(-\log_{10}|\psi_{\mathrm{p}}| - 2.7), 0.172]$$

(McCumber and Pielke, 1981), where ψ_{p} is the moisture potential of soil tension. Clapp and Nornberger (1978) parameterized the moisture potential as

$$\psi_{\mathrm{p}} = \psi_{\mathrm{p,sat}}\left(\frac{w_{\mathrm{sat}}}{w_2}\right)^{b}$$

where $\psi_{\mathrm{p,sat}}$ is the moisture potential when the soil is saturated, w_2 is the volumetric water content of the soil, w_{sat} is the maximum volumetric water content that a given soil type can hold, and b is the slope of the retention curve. The thermal diffusivity is parameterized as

$$\kappa = \frac{k_{\mathrm{s}}}{(1-w_2)\rho_{\mathrm{s}}c_{\mathrm{s}} + w_2\rho_{\mathrm{w}}c_{\mathrm{w}}}$$

where ρ_{s} is the density of the solid soil, c_{s} is the specific heat of the solid soil, and C_{w} is the specific heat of liquid water. Values of $\psi_{\mathrm{p,sat}}$, w_{sat}, b and $\rho_{\mathrm{s}}c_{\mathrm{s}}$ for different soil types can be found in Jacobson (1999).

The value of the air moisture at the lowest level of the model is

$$q(0) = Hu\,q_{\mathrm{sat}}(T_{\mathrm{g}}) \qquad \text{(C5)}$$

where $q_{\mathrm{sat}}(T_{\mathrm{g}})$ is the saturation specific humidity at temperature T_{g}. Hu is the relative humidity related to the near-surface volumetric moisture content by:

$$Hu = \begin{cases} 0.5\left[1-\cos\left(\pi\dfrac{w_{\mathrm{g}}}{w_{\mathrm{fc}}}\right)\right] & \text{if} \quad w_{\mathrm{g}} \le w_{\mathrm{fc}} \\ 1, & \text{otherwise,} \end{cases}$$

where w_{fc} is the field capacity of the soil which corresponds to an hydraulic conductivity of 0.1 mm d^{-1}

it has been estimated for each texture from the soil properties given by Clapp and Nornberger (1978).

The upper boundary conditions have generally been taken from synoptic maps, observations or larger-scale models. In most cases the values for T and q are assumed constant during the day.

$$T(z_{00}) = const, \quad q(z_{00}) = const. \tag{C6}$$

where z_{00} is the highest level of model ($z_{00} = 3025$ m).

C.2. Boundary conditions for carbon dioxide

The lower boundary condition for carbon dioxide is determined primarily by the features of the uppermost soil layer and defined as a flux at the soil surface (upward positive). We used the parameterization for soil respiration according to Lloyd and Farquhar (1994):

$$F^{\uparrow}_{CO_2}(0) = a_{10} \exp\{308.56[1/56.02 - 1/(T_g - 227.13)]\}, \tag{C7}$$

where $F^{\uparrow}_{CO_2}$ is the CO_2 flux in μmol m^{-2} s^{-1}, and a_{10} is the respiration rate at 10 °C.

At the upper border the boundary conditions for the CO_2 concentration can be obtained from measurements and modelling or assumed constant as for T and q

$$C(z_{00}) = const. \tag{C8}$$

C.3. The components of wind speed on the lower and upper boundaries

A no-slip boundary condition is imposed at the lower boundary:

$$u(z = z_0) = v(z = z_0) = w(z = z_0) = 0. \tag{C9}$$

For the upper boundary, the wind components are assumed to be equal to those of the geostrophic wind, viz.

$$u(z = z_{00}) = u_g = G \sin\beta; \quad v(z = z_{00}) = v_g = G \cos\beta, \tag{C10}$$

where β is direction angle of geostrophic wind.

C.4. Turbulent energy on the lower and upper boundaries

No momentum fluxes into the soil and a gradual fading at the upper boundary are assumed:

$$\alpha_e K_z \frac{\partial e}{\partial z}\bigg|_{z=z_0} = 0; \quad e|_{z=z_{00}} = 0. \tag{C11}$$

C.5. The scale of turbulence on the lower boundaries

The closure of the model equations results in a differential equation of the first order for scale of turbulence scale l. Therefore, the turbulence scale needs only one boundary condition. We considered that at small z the scale of turbulence should be asymptotically expressed by the Prandtl formula, hence it is a linear function of height:

$$l(z = z_0) = 0.40 z_0. \tag{C12}$$

Appendix D. Coefficients of water vapour, carbon dioxide and heat exchange at leaves surfaces

To calculate the integral coefficients of water vapour exchange between the surface of phytoelements and air between leaves $g_V^{sn,sd}$ following expression was used:

$$g_V^{sn,sd} = \frac{g_l^{sn,sd} g_{vap}^{sn,sd}}{g_l^{sn,sd} + g_{vap}^{sn,sd}}. \tag{D1}$$

It describes the sequential addition of diffusive resistances for water vapour evaporating from the leaf. In this formula: $g_l^{sn,sd}$ is the sum of cuticular and stomatal conductivity $g_l^{sn,sd} = g_{cut} + g_{st}^{sn,sd}$ and $g_{vap}^{sn,sd}$ represents the water vapour conductivity of the air boundary layer of the phytoelements.

Stomatal conductance is often predicted as a function of environmental factors which directly or indirectly restrict stomata opening below a maximum (g_{max}), so that

$$g_{st}^{sn,sd} = g_{max} f_{PAR}^{sn,sd}(Q_{PAR}) f_T^{sn,sd}(T_l) f_{VPD}^{sn,sd}(VPD) f_w(w_2). \tag{D2}$$

The variables f_{PAR}, f_{VPD}, f_T vary from 0 to 1 and are nonlinear functions of light (Q_{PAR}), leaf temperature

Table 3. *Values of empirical parameters in eqs. (D7) and (D8) to calculate water vapour exchange coefficients*

Re	b_{Re}	m_{Re}	P_{Re}
0–10^3	0.506	0.50	0.6056
10^3–10^5	0.295	0.60	
$>10^5$	0.17	0.84	
Gr	b_{Gr}	m_{Gr}	P_{Gr}
0–1.6×10^{-3}	0.50	0	0.6305
1.6×10^{-3}–800	1.112	0.125	
800–3.2×10^7	0.48	0.25	
$>3.2 \times 10^7$	0.115	0.33	

Table 4. *Values of empirical parameters in eqs. (D10) and (D11) to calculate heat exchange coefficients*

Re	a_{Re}	n_{Re}	P_{Re}
0–10^3	0.528	0.50	0.6056
10^3–10^5	0.352	0.60	
$>10^5$	0.018	0.84	
Gr	a_{Gr}	n_{Gr}	P_{Gr}
0–1.43×10^{-3}	0.50	0	0.6305
$1.43 \times 10^{-3} - 714$	1.128	0.125	
714–2.85×10^7	0.433	0.25	
$>2.85 \times 10^7$	0.120	0.33	

(T_l), and water vapor pressure deficit (VPD), which can be expressed as (Jarvis, 1976):

$$f_{\mathrm{PAR}}^{sn,sd}(Q_{\mathrm{PAR}}) = \frac{Q_{\mathrm{PAR}}^{sn,sd}}{Q_{\mathrm{PAR}}^{sn,sd} + Q_{50}}, \tag{D3}$$

$$f_T^{sn,sd}(T_l) = \frac{\left(T_l^{sn,sd} - T_{\min}\right)\left(T_{\max} - T_l^{sn,sd}\right)^{\Delta}}{(T_{\mathrm{opt}} - T_{\min})(T_{\max} - T_{\mathrm{opt}})^{\Delta}},$$
$$\Delta = (T_{\max} - T_{\mathrm{opt}})/(T_{\mathrm{opt}} - T_{\min}) \tag{D4}$$

$$f_{\mathrm{VPD}}^{sn,sd}(VPD) = 1\Big/\left(1 + \alpha_{\mathrm{V}}\, VPD^{sn,sd}\right) \tag{D5}$$

where $Q_{\mathrm{PAR}}^{sn,sd}$ is incoming photosynthetically active radiation for sunlit and shaded leaves, respectively, and Q_{50} is the value of Q_{PAR} when $g_{st} = g_{\mathrm{st}}^{\max}/2$; T_{opt}, $T_{\min}$ and $T_{\max}$ are optimal leaf temperature and lower and upper leaf temperature limits for stomatal conductivity; $\alpha_{\mathrm{V}} = 0.67$ is an empirical constant. The influence of such factors as available soil water f_{w} has been estimated as follow (Jacquemin and Noilhan, 1990)

$$f_{\mathrm{w}}(w_2) = \frac{w_2 - w_{\mathrm{wilt}}}{w_{\mathrm{fc}} - w_{\mathrm{wilt}}} \quad \text{and} \quad 0 \le f_{\mathrm{w}} \le 1. \tag{D6}$$

w_{wilt} is the wilting point volumetric moisture for given type of soil texture. The influences of ambient CO_2 concentrations and air pollutants on stomata are not described in the present model.

The water exchange between the leaf surface and the between-leaves air occurs under the condition of forced or free convection regime. The choice of the conditions assumed in each particular case is made by comparing Reynolds (Re) and Grasshoff (Gr) criteria. It has been assumed in our model that the forced convection is realized in the case when $\mathrm{Re}^2 = \mathrm{Gr}$ (Menzhulin, 1986). To describe $g_{vap}^{sn,sd}$ for forced convection it is convenient to use the following formulas:

$$g_{vap}^{sn,sd} = \frac{\chi_{\mathrm{V}}}{d_l P_{\mathrm{Re}}}\mathrm{Sh}_{\mathrm{Re}}, \quad \mathrm{Sh}_{\mathrm{Re}} = b_{\mathrm{Re}}\mathrm{Re}^{m_{\mathrm{Re}}}. \tag{D7}$$

In the conditions of free convection $g_{vap}^{sn,sd}$ is

$$g_{vap}^{sn,sd} = \frac{\chi_{\mathrm{H}}}{d_l P_{\mathrm{Gr}}}\mathrm{Sh}_{\mathrm{Gr}}, \quad \mathrm{Sh}_{\mathrm{Gr}} = b_{\mathrm{Gr}}\mathrm{Re}^{m_{\mathrm{Gr}}}. \tag{D8}$$

In these expressions d_l is the characteristic linear size of the phytoelements and χ_{V} is the molecular diffusivity of water vapour. The empirical parameters included into the formulas for $g_{vap}^{sn,sd}$ are given in Table 3.

To calculate the integral exchange coefficients for CO_2 between the surface of phytoelements and air between the leaves $g_{\mathrm{C}}^{sn,sd}$, we took in account differences in conductance between CO_2 and water vapour for stomata (factor 0.625) and air boundary layer on the phytoelements (factor 0.748) (Campbell and Norman, 1998), thus:

$$g_{\mathrm{C}}^{sn,sd} = \frac{0.625 g_l^{sn,sd} \times 0.748 g_{vap}^{sn,sd}}{0.625 g_l^{sn,sd} + 0.748 g_{vap}^{sn,sd}}. \tag{D9}$$

For the heat exchange coefficients for phytoelements the following expressions have been used in our model:

In the case of forced convection:

$$g_{\mathrm{H}}^{sn,sd} = \frac{\chi_{\mathrm{H}}}{d_l P_{\mathrm{Re}}}\mathrm{Nu}_{\mathrm{Re}}, \quad \mathrm{Nu}_{\mathrm{Re}} = a_{\mathrm{Re}}\mathrm{Re}^{n_{\mathrm{Re}}}. \tag{D10}$$

In the case of free convection:

$$g_{\mathrm{H}}^{sn,sd} = \frac{\chi_{\mathrm{H}}}{d_l P_{\mathrm{Gr}}}\mathrm{Nu}_{\mathrm{Gr}}, \quad \mathrm{Nu}_{\mathrm{Gr}} = a_{\mathrm{Gr}}\mathrm{Re}^{n_{\mathrm{Gr}}}, \tag{D11}$$

In these expressions χ_{H} is the molecular thermal diffusivity. The parameter values included in these formulas are presented in Table 4.

REFERENCES

Alapaty, K., Raman, S. and Niyogi, S. 1997. Uncertainty in the specification of surface characteristics: a study of prediction errors in the boundary layer. *Boundary-Layer Meteorol*. **82**, 473–500.

Apsley, D. and Castro, I. 1997. A limited-length-scale k-e model for the neutral and stably-stratified atmospheric boundary layer. *Boundary-Layer Meteorol*. **83**, 75–98.

Ayotte, K., Finnigan, J. and Raupach, M. 1999. A second-order closure for neutrally stratified vegetative canopy flows. *Boundary-Layer Meteorol*. **90**, 189–216.

Belov, P., Borisenkov, E. and Panin, B. 1989. *Numerical methods of weather forecast*. Hydrometeoizdat, Moscow, 376 pp (in Russian).

Belsky, A. J., Amundson, R. G., Duxbury, J. M., Riha, S. J., Ali, A. R. and Mwonga, S. M. 1989. The effects of trees on their physical, chemical and biological environments in a semi-arid savanna in Kenya. *J. Appl. Ecol*. **26**, 1005–1024.

Blakadar, A. K. 1962. The vertical distrubution of wind and turbulent exchange in a neutral atmosphere. *J. Geophys. Res*. **67**, 3095–3102.

Bobylyeva, I. 1970. The study of turbulence characteristics in the atmospheric boundary layer. *Trans. Leningrad Hydrometeorol. Inst*. **40**, 3–63 (in Russian).

Brown, A. R. 1996. Evaluation of parametrization schemes for the convective boundary layer using large-eddy simulation results. *Boundary-Layer Meteorol*. **81**, 167–200.

Businger, J., Wyngaard, J. C., Izumi, Y. and Bradley, E. F. 1971. Flux-profile relationships in the atmospheric surface layer. *J. Atmos. Sci*. **28**, 181–189.

Campbell, G. S. and Norman, J. M. 1988. *Environ. Biophys*. Springer, Berlin, 286 pp.

Carroll, J. 1993. Sensitivity of PBL model predictions to model design and uncertainties in environmental inputs. *Boundary-Layer Meteorol*. **65**, 137–158.

Clapp, R. B. and Nornberger, G. M. 1978. Empirical equations for some soil hydraulic properties. *Water Resour. Res*. **14**, 601–604.

Cowan, I. R. and Farquhar, G. D. 1977. Stomatal function in relation to leaf metabolism and environment. *Symp. Soc. Exper. Biol*. **31**, 471–505.

Cowan, I. R. 1977. Stomatal behavior and environment. *Adv. Bot. Res*. **4**, 117–228.

DePury, D. and Farquhar, G. D. 1997. Simple scaling of photosynthesis from leaves to canopies without the errors of big-leaf models. *Plant, Cell Environ*. **20**, 537–557.

Dubov, A. and Bykova, L. 1973. Characteristics of turbulent flow in atmospheric boundary layer over forest and inside it. *Trans. Main Geophys. Observatory* **297**, 13–24 (in Russian).

Dubov, A., Bykova, A. and Marunich, C. 1978. *Turbulence in vegetation canopy*. Hydrometeoizdat, Leningrad. 182 pp (in Russian).

Finnigan, J. 2000. Turbulence in plant canopies. *Annu. Rev. Fluid Mech*. **32**, 519–571.

Garratt, J. R., Hess, G. D., Physick, W. L. and Bougeault, P. 1996. The atmospheric boundary layer – advances in knowledge and application. *Boundary-Layer Meteorol*. **78**, 9–37.

Gross, G. 1987. Some effects of deforestation on nocturnal drainage flow and local climate: a numerical study. *Boundary-Layer Meteorol*. **38**, 315–337.

Gross, G. 1993. *Numerical simulation of canopy flows*, Springer Verlag, Berlin, 168 pp.

Gutman, L. 1969. The introduction to the nonlinear theory of mesometeorological processes. Gidrometeoizdat, Leningrad. 229 pp (in Russian).

Hasse, L. 1993. Turbulence closure in boundary-layer theory – an invitation to debate. *Boundary-Layer Meteorol*. **65**, 249–254.

Jacobson, M. Z. 1999. *Fundamentals of atmospheric modeling*. Cambridge University Press, Cambridge, 656 pp.

Jacquemin, B. and Noilhan, J. 1990. Sensitivity study and validation of a land surface parameterization using the HAPEX-MOBILHY data set. *Boundary-Layer Meteorol*. **52**, 93–134.

Jarvis, P. G. 1976. The interpretation of the variations in leaf water potential and stomatal conductance found in canopies in the field. *Philos. Trans. R. Soc. London, Ser. B* **273**, 593–610.

Kalnay, E., et. al. 1996. The NCEP/NCAR 40-year reanalysis project, *Bull. Am. Meteorol. Soc*. **77**, 437–471.

Kanda, M. and Hino, M. 1994. Organized structures in development turbulent flow within and above a plant canopy, using a large eddy simulation. *Boundary-Layer Meteorol*. **68**, 237–257.

Karpov, V. 1983. *Regulation factors of spruce forest ecosystem,* Nauka, Leningrad. 320 pp (in Russian).

Kelliher, F. M., Lloyd, J., Arneth, A., Byers, J. N., McSeveny, T. M., Milukova, I., Grigoriev, S., Panfyorov, M., Sogatchev, A., Varlagin, A., Ziegler, W., Bauer, G. and Schulze, E.-D. 1988. Evaporation from a central Siberian Forest. *J. Hydrol*. **205**, 279–296.

Kolmogorov, A. 1941. A local turbulence structure in uncompressible fluids at very high Reynold's numbers. *Rep. USSR Acad. Sci*. **30**, 299–303 (in Russian).

Kolmogorov, A. 1942. Turbulence flow equations of an uncompressible fluid. *Trans. USSR Acad. Sci. Phys*. **6**, 56–58 (in Russian).

Kondratev, K. Ya. 1954. *Radiation in the Atomsphere*. Hydrometeoizdat, Leningrad. 600 pp (in Russian).

Kunz, R. and Moussiopoulos, N. 1995. Simulation of the wind fields in Athens using refined boundary conditions. *Atmos. Environ*. **29**, 3575–3591.

Kunz, R. and Moussiopoulos, N. 1997. Implementation and assessment of a one-way nesting technique for high resolution wind flow simulation. *Atmos. Environ*. **31**, 3167–3176.

Laykhtman, D. 1970. Physics of atmospheric boundary layer. Gidrometeoizdat, Leningrad, 341 pp (in Russian).

Leclerc, M. Y. and Thurtell, G. W. 1990. Footprint predictions of scalar fluxes using a marcovian analysis. *Boundary-Layer Meteorol*. **52**, 247–258.

Legotina, S. I. and Orlenko, L. R. 1977. On turbulent flow calculations of sensible and latent heat using gradient measurements data. *Trans. Main Geophys. Observatory* **398**, 91–98 (in Russian).

Liu, J., Chen, J. M., Black, T. A. and Novak, M. D. 1996. E-e modelling of turbulent air flow downwind of a model forest edge. *Boundary-Layer Meteorol*. **77**, 21–44.

Lloyd, J. and Farquhar, G. D. 1994. ^{13}C discrimination during CO_2 assimilation by the terrestrial biosphere. *Oecologia* **99**, 210–215.

Lloyd, J. and Taylor, J. A. 1994. On the temperature dependence of soil respiration. *Funct. Ecol*. **8**, 315–323.

Lloyd, J., Grace, J., Miranda, A. C., Meir, P., Wong, S. C., Miranda, H. S., Wright, I. R., Gash, J. H. C. and McIntyre, J. 1995. A simple calibrated model of Amazon rainforest productivity based on leaf biochemical properties. *Plant, Cell Environ*. **18**, 1129–1145.

Lloyd, J., Francey, R. J., Mollicone, D., Raupach, M. R., Sogachev, A., Arneth, A., Byers, J. N., Kelliher, F. M., Rebmann, C., Valentini, R., Wong, S.-C., Bauer, G. and Schulze, E.-D. 2001. Vertical profiles, boundary layer budgets, and regional flux estimates for CO_2, its $^{13}C/^{12}C$ ratio and for water vapour above a forest/bog mosaic in central Siberia *Global Biogeochem. Cycles* **15**, 267–284.

Lloyd, J., Langenfelds, R., Francey, R. J., Gloor, M., Zolotikine, D., Tchebakova, N., Shibistova, O., Allison, C. A., Brand, W. A., Werner, R. and Schulze, E.-D. 2002. A trace gas climatology above Zotino, central Siberia *Tellus* **54B**, this issue.

McCumber, M. C. and Pielke, R. A. 1981. Simulation of the effects of surface fluxes of heat and moisture in a mesoscale numerical model. Part I: Soil layer. *J. Geophys. Res*. **86**, 9929–9938.

Mellor, G. and Yamada, T. 1975. A simulation of the Wangara atmospheric boundary layer data. *J. Atmos. Sci*. **32**, 2309–2329.

Menzhulin, G. 1970. On the calculation methodology of the meteorological regime in vegetation canopies. *Meteorol. Hydrol*. **2**, 92–99 (in Russian).

Menzhulin, G. 1974. Modeling of the hydrometeorological regime in vegetations. *Trans. Main Geophys. Observatory* **318**, 5–34 (in Russian).

Menzhulin, G. 1986. Energy and matter transfer in agroecosystems. D. Sci. Thesis, Leningrad State Hydrological Institute, 507 pp (in Russian).

Mix, W., Goldberg, V. and Bernhardt, K.-H. 1994. Numerical experiments with different approaches for boundary layer modeling under large-area forest canopy conditions. *Meteorol. Z*. **3**, 187–192.

Monin, A. and Yaglom, A. 1965. *Statistical hydromechanics. Part 1*, Science Publ., Moscow, 640 pp (in Russian).

Monteith, J. L. and Unsworth, M. H. 1990. *Principles of environmental physics* (2nd edn.). Edward Arnold London, 291 pp.

Naegler, T., Kolle, O., Milukova, I., Varlagin, A. and Levin, I. 2002. Comparison of methods to measure nocturnal respirative CO_2 fluxes in a temperate forest in Western Russia. *Tellus* **54B**, this issue.

Nichols, W. D. 1992. Energy budgets and resistance to energy transport in sparsely vegetated rangeland. *Agric. Forest Meteorol*. **60**, 221–247.

Nickerson, E. C. and Smiley, V. E. 1975. Surface energy budget parameterizations for urban scale models. *J. Appl. Meteorol*. **14**, 297–300.

Noilhan, J. and Planton, S. 1989. A simple parameterization of land surface processes for meteorological model. *Mon. Wea. Rev*. **117**, 536–549.

Penenko, V. and Aloyan, A. 1985. Models and methods for environmental protection problems. Science Publ, Moscow, 256 pp (in Russian).

Pielke, R. 1984. *Mesoscale meteorological modeling*. Academic Press, New York, 612 pp.

Rannic, Ü., Aubinet, M., Kurbanmuradov, O., Sabelfeld, K. K., Markkanen, T. and Vesala, T. 2000. Footprint analysis for measurements over a heterogeneous forest. *Boundary-Layer Meteorol*. **97**, 137–166.

Raupach, M. R. 1995. Vegetation-atmosphere interaction and surface conductance at leaf, canopy and regional scales. *Agric. Forest Meteorol*. **73**, 151–179.

Raupach, M. R., Finnigan, J. J. and Brunet, Y. 1996. Coherent eddies and turbulence in vegetation canopies: the mixing-layer analogy. *Boundary-Layer Meteorol*. **78**, 351–382.

Ross, Yu. K. 1975. Radiation regime and architecture of vegetation canopies. Gidrometeoizdat, Leningrad, 342 pp (in Russian).

Ross, Yu. K. and Nilson, T. A. 1967. The radiation regime of a vegetation canopy with horizontally oriented leaves. In *Phytoactinometrical researches of vegetation canopy*. Valgus Publ. Tallin, 5–34 (in Russian).

Schilling, V. 1991. A parameterization for modelling the meteorological effects of tall forest – a case study of a large clearing. *Boundary-Layer Meteorol*. **55**, 283–304.

Schulze, E.-D., Lloyd, J., Kelliher, F. M., Wirth, C., Rebmann, C., Lühker, B., Mund, M., Knohl, A., Milykova, I., Schulze, W., Ziegler, W., Varlagin, A., Valentini, R., Sogachov, A., Valentini, R., Dore, S., Grigoriev, S., Kolle, O., Tchebakova, N. and Vygodskaya, N. N. 1999. Productivity of forests in the Eurosiberian boreal region and their potential to act as a carbon sink – A synthesis. *Global Change Biol*. **5**, 703–722.

Sellers, P., Mintz, Y., Sud, V. and Dalcher, A. 1986. A simple model (Si-B) for use within general circulation models. *J. Atmos. Sci*. **43**, 505–531.

Shaw, R. and Schumann, U. 1992. Large eddy eimulation of turbulent flow above and within a forest. *Boundary-Layer Meteorol*. **61**, 47–64.

Shen, S. and Leclerc, M. Y. 1997. Modelling the turbulent structure in the canopy layer. *J. Agric. Forest Meteorol*. **87**, 3–25.

Shibistova, O., Lloyd, J., Kolle, O., Arneth, A. and Schulze, E.-D. 2002. Seasonal and spatial variability in soil CO_2 efflux rates for a central Siberian *Pinus sylvestris* forest. *Tellus* **54B**, this issue.

Sivkov, S. I. 1968. Calculation methods of solar radiation characteristics. Gidrometeoizdat, Leningrad, 232 pp (in Russian).

Smagorinsky, J. 1965. General circulation experiments with the primitive equations: The basic experiment. *Mon. Wea. Rev.* **93**, 727–760.

Sorbjan, Z. 1989. *Structure of the atmospheric boundary layer*. Prentice-Hall, and Englewood Cliffs, NJ, 360 pp.

Spitters, C. J. T., Toussaint, H. A. J. M. and Goudriaan, J. 1986. Separating the diffuse and direct component of global radiation and its implications for modelling canopy photosynthesis: Part I. Components of incoming radiation. *J. Agric. For. Meteorol.* **38**, 217–229.

Stull, R. B. 1988. An introduction to boundary layer meteorology. Kluver Academic Publishers, Dordrecht, 670 pp.

Styles, J. M., Lloyd, J., Zolotukhin, D., Kieran, A., Lawton, Tchebakova, N., Francey, R. J., Arneth, A., Salamakho, D., Kolle, O. and Schulze, E.-D. 2002. Estimates of regional surface carbone and oxygen isotope discrimination during photosynthesis from profile of CO_2 concentration and its isotopic composition in the convective boundary layer. *Tellus* **54B**, this issue.

Sun, W.-Y. and Bosilovich, W. 1996. Planetary boundary layer and surface layer sensitivity to land surface parameters. *Boundary-Layer Meteorol.* **77**, 353–378.

Therry, G. and Lacarrere, P. 1983. Improving the eddy kinetic energy model for planetary boundary layer description. *Boundary-Layer Meteorol.* **25**, 63–88.

Tjernström, M. 1989. Some tests with a surface energy balance scheme, including a bulk parameterization for vegetation in a mesoscale model. *Boundary-Layer Meteorol.* **48**, 33–68.

Tsipris, I. B. and Menzhulin, G. V. 1972. The calculation of relationship between forest belts and surface airflow. *Meteorol. Hydrol.* **N11**, 82–88 (in Russian).

Tuzet, A., Perrier, A., and Olid Aissa, A. K. 1993. A prediction model for field drying of hay using a heat balance method. *Agric. Forest Meteorol.* **65**, 63–89.

Vager, B. and Nadezhina, E. 1975. A model for the turbulence scale and calculations of the atmospheric boundary layer structure. *Trans. Main Geophys. Observatory* **326**, 3–10. (in Russian).

Vager, B. and Nadezhina, E. 1979. Atmospheric boundary layer in conditions of horizontal nonuniformity. Gidrometeoizdat, Leningrad, 136 pp (in Russian).

Valentini, R., Dore, S., Marchi, G., Mollicone, D., Panfyorov, M., Rebmann, C., Kolle, O. and Schulze, E.-D. 2000. Carbon and water exchanges of two contrasting central Siberia landscape types: regenerating forest and bog. *Funct. Ecol.* **14**, 87–96.

Varlagin, A. V. and Vygodskaya, N. N. 1993. Influence of ecological and morphological factors on stomata resistance of norway spruce. Lesovedenie, Moscow **3**, 48–60. (in Russian).

Wang, H., Takle, E. S. and Shen, J. 2001. Shelterbelts and windbreaks: Mathematical modeling and computer simulation of turbulent flows. *Annu. Rev. Fluid Mech.* **33**, 549–586.

Wang, Y. P. and Leuning, R. 1998. A two-leaf model for canopy conductance, photosyntesis and partioning of available energy. Part I: Model description and comparison with a multi-layered model. *Agric. For. Meteorol.* **91**, 89–111.

Wilson, J. 1988. A second-order closure model for flow through vegetation. *Boundary-Layer Meteorol.* **42**, 371–392.

Wilson, J. and Flesch, T. 1999. Wind and remnant tree sway in forest cutblocks. Part 3. A windflow model to diagnose spatial variation. *Agric. For. Meteorol.* **93**, 259–282.

Wu, J., Liu, Y. and Jelinski, D. 2000. Effects of leaf area profiles and canopy stratification on simulated energy fluxes: the problem of vertical spatial scale. *Ecol. Modelling* **134**, 283–297.

Zeng, P. and Takahashi, H. 2000. A first-order closure model for wind flow within and above vegetation canopies. *Agric. For. Meteorol.* **103**, 301–313.

Zhenjia, L. I., Lin, J. D. and Miller, D. R. 1990. Air flow over and through a forest edge: a steady-state numerical simulation. *Boundary-Layer Meteorol.* **51**, 179–197.

Ziemann, A. 1998. Numerical simulation of meteorological quantities in and above forest canopies. *Meteorol. Z.* **7**, 120–128.

Zilitinkevich, S. 1970. *Dynamics of the atmospheric boundary layer*. Gidrometeoizdat, Leningrad, 291 pp (in Russian).